Gating and Conductance Properties of BK Channels Are Modulated by the S9–S10 Tail Domain of the α Subunit

A Study of mSlo1 and mSlo3 Wild-type and Chimeric Channels

Brenda L. Moss and Karl L. Magleby

Department of Physiology and Biophysics, University of Miami School of Medicine, Miami, FL 33101

ABSTRACT The COOH-terminal S9–S10 tail domain of large conductance Ca^{2+}-activated K^+ (BK) channels is a major determinant of Ca^{2+} sensitivity (Schreiber, M., A. Wei, A. Yuan, J. Gaut, M. Saito, and L. Salkoff. 1999. *Nat. Neurosci.* 2:416–421). To investigate whether the tail domain also modulates Ca^{2+}-independent properties of BK channels, we explored the functional differences between the BK channel mSlo1 and another member of the Slo family, mSlo3 (Schreiber, M., A. Yuan, and L. Salkoff. 1998. *J. Biol. Chem.* 273:3509–3516). Compared with mSlo1 channels, mSlo3 channels showed little Ca^{2+} sensitivity, and the mean open time, burst duration, gaps between bursts, and single-channel conductance of mSlo3 channels were only 32, 22, 41, and 37% of that for mSlo1 channels, respectively. To examine which channel properties arise from the tail domain, we coexpressed the core of mSlo1 with either the tail domain of mSlo1 or the tail domain of mSlo3 channels, and studied the single-channel currents. Replacing the mSlo1 tail with the mSlo3 tail resulted in the following: increased open probability in the absence of Ca^{2+}; reduced the Ca^{2+} sensitivity greatly by allowing only partial activation by Ca^{2+} and by reducing the Hill coefficient for Ca^{2+} activation; decreased the voltage dependence ~28%; decreased the mean open time two- to threefold; decreased the mean burst duration three- to ninefold; decreased the single-channel conductance ~14%; decreased the K_d for block by TEA_i ~30%; did not change the minimal numbers of three to four open and five to seven closed states entered during gating; and did not change the major features of the dependency between adjacent interval durations. These observations support a modular construction of the BK channel in which the tail domain modulates the gating kinetics and conductance properties of the voltage-dependent core domain, in addition to determining most of the high affinity Ca^{2+} sensitivity.

KEY WORDS: Ca^{2+}-activated K^+ channel • maxi K^+ channel • TEA • MWC model • gating kinetics

INTRODUCTION

Large-conductance Ca^{2+}-activated potassium channels (BK channels)* are activated by both intracellular Ca^{2+} and membrane depolarization. Consequently, BK channels can provide a direct link between Ca^{2+}-dependent cellular processes and membrane excitability (for reviews see McManus, 1991; Latorre, 1994; Conley, 1996; Kaczorowski et al., 1996). Through this process, BK channels modulate neurotransmitter release (Robitaille et al., 1993), secretion in both endocrine and exocrine cells (Petersen and Maruyama, 1984), smooth muscle contraction (Nelson et al., 1995), and the electrical tuning of cochlear hair cells (Hudspeth and Lewis, 1988; Wu et al., 1995).

The cloning of BK channels has paved the way toward approaching an understanding of the molecular mechanism of activation. The cDNAs encoding the pore-forming α subunit were first obtained from *Drosophila* (dSlo; Atkinson et al., 1991; Adelman et al., 1992) and later from additional species including mouse (mSlo1; Butler et al., 1993; Pallanck and Ganetzky, 1994), chick (cSlo; Jiang et al., 1997; Navaratnam et al., 1997; Rosenblatt et al., 1997), and human (hSlo; Dworetzky et al., 1994; Pallanck and Ganetzky, 1994; Tseng-Crank et al., 1994; McCobb et al., 1995). Alignment of the predicted primary sequences as well as structure–function studies have shown that the BK channel α subunit can be divided into two domains: (1) a core domain and (2) a COOH-terminal tail domain (Wei et al., 1994). The core domain (hydrophobic segments S0–S8) includes six putative transmembrane segments (S1–S6) similar to the pore-forming subunits in the S4 superfamily of voltage-gated K^+ channels (such as *Shaker*). As in the S4 superfamily, the S4 segment in BK channels has been shown to play a major role in sensing voltage (Diaz et al., 1998; Cui and Aldrich, 2000). The additional transmembrane segment (S0) is

The present address of Dr. Moss is Department of Biological Sciences, Purdue University, West Lafayette, IN 47907.

Address correspondence to Karl L. Magleby, Ph.D., Department of Physiology and Biophysics, University of Miami School of Medicine, P.O. Box 016430, Miami, FL 33101-6430. Fax: (305) 243-6898; E-mail: kmagleby@miami.edu

**Abbreviations used in this paper:* 2-D, two dimensional; BK channel, large-conductance Ca^{2+}-activated K^+ channel; MWC, Monod-Wyman-Changeux; P_O, open probability.

required for modulation by the β subunit (Wallner et al., 1996). The COOH-terminal tail domain (S9–S10) is intracellular (Meera et al., 1997) and plays a key role in sensing Ca^{2+} (Wei et al., 1994; Schreiber and Salkoff, 1997; Schreiber et al., 1998, 1999). Two separate regions of the tail domain appear to be critical for Ca^{2+} sensing: the calcium bowl located between S9 and S10, which includes a string of aspartate residues, and a region which is adjacent to the calcium bowl and includes S10 (Schreiber and Salkoff, 1997; Schreiber et al., 1999). Consistent with these findings, a recent study of the dSlo channel has demonstrated Ca^{2+} binding activity using a COOH-terminal fragment that includes both Ca^{2+}-sensing regions (Bian et al., 2001), and a bacterially expressed protein encompassing site 6 of mSlo, which includes the calcium bowl, could directly bind Ca^{2+} (Braun and Sy, 2001).

The purpose of our present study is to further define the functional role of the COOH-terminal tail domain. Its role as the primary Ca^{2+} sensor requires that there be an interaction between the core and tail domains so that Ca^{2+} binding can regulate channel gating (Schreiber et al., 1999). Such an interaction suggests that the tail domain also may modulate other channel properties that are typically associated with the core domain. To explore this possibility, we examined the effect of the tail domain on the bursting kinetics, the voltage dependence, the single-channel conductance, and the sensitivity to block by internal TEA. We took advantage of the functional differences between the BK channel mSlo1 and another recently identified member of the Slo family of K^+ channels, mSlo3, which is a pH-sensitive K^+ channel from mammalian spermatocytes (Schreiber et al., 1998). Compared with mSlo1, mSlo3 is Ca^{2+}-insensitive, has a briefer mean open time, and a lower single-channel conductance.

Previous experiments have shown that the separate core (S0–S8) and tail (S9–S10) domains of BK channels expressed by themselves do not form functional channels (Wei et al., 1994; Meera et al., 1997), but when coexpressed, they assemble to form functional channels with properties like the wild-type channels (Wei et al., 1994; Meera et al., 1997). Schreiber et al. (1999) have shown that coexpression of the mSlo1 core with the mSlo3 tail yields macroscopic currents that are voltage-activated and Ca^{2+}-insensitive, which is consistent with the mSlo1 tail domain as the major Ca^{2+} sensor. To determine what other functional properties are contributed by the tail domain, we used single-channel recording to study wild-type mSlo1 and wild-type mSlo3 channels and also channels expressed from the mSlo1 core domain together with either the mSlo1 tail domain (mSlo1 tail channels) or the mSlo3 tail domain (mSlo3 tail channels).

Consistent with the findings of Schreiber et al. (1999), we found that replacing the mSlo1 tail with the mSlo3 tail resulted in a drastic reduction in Ca^{2+} sensitivity as well as an increase in open probability in the absence of Ca^{2+}. In addition, compared with channels with mSlo1 tails, we found that channels with mSlo3 tails showed decreases in the voltage dependence, mean open time, number of openings per burst, burst duration, and single-channel conductance, as well as an increase in sensitivity to block by internal TEA. These results suggest that, in addition to playing a key role in sensing Ca^{2+}, the COOH-terminal tail domain of the BK channel also modulates the gating and conductance properties of the channel. In addition, we found that the removal of the major Ca^{2+} binding site from mSlo1 BK channels through the replacement of the mSlo1 tail with the mSlo3 tail did not change the minimal estimates of three to four open and five to seven kinetic states entered during gating. This observation is consistent with the large multitiered state models that have been proposed for the gating of BK channels (Rothberg and Magleby, 1999, 2000; Cui and Aldrich, 2000), where a tetrameric voltage-dependent gating mechanism is modulated by Ca^{2+} binding, and argues against simpler models, such as the Monod-Wyman-Changeux (MWC) model (Monod et al., 1965).

Portions of this work were previously published in abstract form (Moss and Magleby, 2000).

MATERIALS AND METHODS

Expression of Cloned Channels in Xenopus Oocytes

Constructs encoding wild-type mSlo1 and mSlo3 channels, as well as the separate mSlo1 core domain, and the separate mSlo1 and mSlo3 tail domains were a gift from Dr. Lawrence Salkoff and Dr. Matthew Schreiber (Washington University School of Medicine, St. Louis, MO). Details on the constructs can be found in Schreiber et al. (1999). Capped cRNAs were transcribed in vitro using the mMessage mMachine kit (Ambion) and resuspended in nuclease-free water at a final concentration of ~1 μg/μl. The mSlo1 core cRNA was then mixed 1:1 (vol/vol) with either the mSlo1 tail or mSlo3 tail cRNA. Because the cRNA encoding the core domain is about two to three times longer than the cRNA encoding either tail domain, the tail domain cRNA was in about two- to threefold molar excess over the core domain cRNA.

Xenopus laevis oocytes were separated enzymatically using collagenase as previously described (Dahl, 1992) and microinjected with 40–50 nl of cRNA encoding mSlo1 core and mSlo1 tail (~1–5 ng of each cRNA; total of ~2–10 ng/oocyte) or mSlo1 core and mSlo3 tail (~5–25 ng of each cRNA; total of ~10–50 ng/oocyte). We found that the mSlo3 tail channels typically did not express as well as the mSlo1 tail channels, and, therefore, required microinjection of a larger amount of cRNA. In experiments examining the properties of wild-type channels, oocytes were microinjected with 0.8 ng for wild-type mSlo1or 40–70 ng for wild-type mSlo3. Coinjection of mSlo3 core domains with mSlo1 tail domains does not produce functional channels (Schreiber et al., 1999), so this combination was not studied.

Although we have not demonstrated directly that all channels studied were comprised of both core and tail domains, several lines of evidence suggest that this was the case. First, no functional BK channels were detected in patches from oocytes injected with

only mSlo1 core cRNA (~75 ng/oocyte). This observation is consistent with results of Wei et al. (1994) showing that the mSlo1 core alone produced no detectable currents, as assayed by both whole-cell and single-channel recordings. Second, Meera et al. (1997) found that expression of the core domain or the tail domain by themselves do not form functional channels, so that the functional channels that we observed must include both core and tail domains. Third, since the tail domain forms a freely diffusible cytoplasmic protein (Meera et al., 1997), if the tails dissociated during the experiment, then the tail would be expected to diffuse away from excised patches, and channel activity would be expected to cease. The observed numbers of active channels in a patch seldom changed during an experiment, suggesting that dissociation and diffusion did not occur. Fourth, Wei et al. (1994) found that channels resulting from coinjection of separate mSlo1 cores and mSlo1 tails produced channels that were essentially indistinguishable from their full-length counterparts, and we found (see RESULTS) similar bursting kinetics for channels expressed in these two different ways. Similar kinetics of channels expressed from full-length subunits and from separate cores and tails suggests that the mSlo1 cores and tails assembled to form channels with function (and presumably structure) similar to the wild-type channels. These observations argue against the possibility that the separate cores and tails were functionally altered by proteases or that fewer than four tail domains associate with each mSlo1 channel. Finally, channels coexpressed from mSlo1 core domains and mSlo3 tail domains (mSlo3 tail channels) exhibited markedly different bursting kinetics from channels coexpressed from mSlo1 core domains and mSlo1 tail domains (mSlo1 tail channels), suggesting that the mSlo1 core and the mSlo3 tail also assembled to form functional channels. Although we cannot establish that every mSlo1 tail channel and every mSlo3 tail channel that we studied contained four tail domains, the above observations and the excess injection of the cRNA for the tail domains would suggest four tail domains per channel.

Single-channel Recording

Currents were recorded from wild-type mSlo1, wild-type mSlo3, mSlo1 tail, and mSlo3 tail channels expressed separately in *Xenopus* oocytes 2–4 d after injection using the inside-out configuration of the patch-clamp technique (Hamill et al., 1981). To reduce noise, patch pipettes were coated with Sigmacote (Sigma-Aldrich), and only the very tip of the recording electrode was placed in solution. Currents were recorded with an Axopatch 200B amplifier (Axon Instruments, Inc.). Unless otherwise indicated, experiments were performed on patches containing a single channel, determined by extended recordings at high levels of Ca^{2+} or depolarized potentials expected to readily activate the channels. *Xenopus* oocytes can express very low levels of endogenous BK channels (Krause et al., 1996). Consequently, we cannot exclude that we might have recorded from such channels. However, we have not yet observed BK channels in patches pulled from uninjected oocytes, or in oocytes with only the core domain injected, and the channels we did record from had properties that would be expected for the various combinations of the core and tail domains. Experiments were performed at room temperature (21–24°C).

In all experiments, the extracellular solution contained 150 mM KCl, 5 mM TES [*N*-Tris(hydroxymethyl)methyl-2-aminoethane sulfonic acid] pH buffer and 100 μM $GdCl_3$ to block endogenous mechanosensitive channels (Yang and Sachs, 1989). The intracellular solution contained 150 mM KCl and 1 mM EGTA to buffer the Ca^{2+}, 5 mM TES, and either no added Ca^{2+} or sufficient $CaCl_2$ to achieve the indicated levels of free Ca^{2+}. The free Ca^{2+} was estimated by calibration against previous experiments (Nimigean and Magleby, 1999) so that direct comparisons of results could be made. Unless otherwise indicated, solutions were adjusted to pH 7.0. For experiments with no added Ca^{2+} and 1 mM EGTA, the estimated free Ca^{2+} was $<10^{-8}$ M. These solutions will be referred to as 0 Ca^{2+} solutions, as Ca^{2+} at this low concentration has little, if any, effect on channel gating (Meera et al., 1996; Nimigean and Magleby, 2000). For some experiments comparing burst kinetics between wild-type mSlo1 and wild-type mSlo3 channels, the bath solution was adjusted to pH 7.4 to increase the level of activity of the pH-dependent wild-type mSlo3 channels. For the experiments with TEA, the internal TEA concentration (TEA_i) was increased while the concentration of KCl was maintained at 150 mM, as described in Blatz and Magleby (1984).

Analysis of Single-channel Recordings

In experiments measuring specific kinetic parameters that are highly sensitive to differences in filtering (such as mean open time and the mean number of openings per burst), current records were low-pass filtered with a 4-pole Bessel filter to give a final effective filtering of 7–8 kHz (−3 dB). In experiments in which the parameters of interest were relatively insensitive to the level of filtering (such as single-channel conductance and open probability [P_O]), current records were low-pass filtered to give a final effective filtering of 3–8 kHz. Single-channel currents were first recorded on a digital data recorder (DC-37 kHz), and after additional filtering (as described in this paragraph) were sampled by computer at a rate of 200 kHz.

The methods used to measure interval durations with half-amplitude threshold analysis and to use stability plots to identify data with stable channel activity for analysis and also to exclude data during mode shifts have been described previously (McManus and Magleby, 1988; 1991; Silberberg et al., 1996; Moss et al., 1999). For wild-type mSlo1 channels and for mSlo1 tail channels, the most common mode observed was the normal mode, which typically accounts for ~96% of the detected intervals in BK channels from cultured rat skeletal muscle (McManus and Magleby, 1988). In addition to the normal mode activity, wild-type mSlo1 channels, mSlo1 tail channels, and mSlo3 tail channels could enter a Ca^{2+}-dependent low activity mode and also Ca^{2+}-independent isolated long shut intervals (Rothberg et al., 1996). Both of these modes were removed before analysis. For wild-type mSlo3 channels, only one apparent mode was observed. In some experiments, the wild-type mSlo3 channels showed a decrease in channel activity (rundown) over several minutes, as described by Schreiber et al. (1998). These experiments were excluded from analysis. For some patches, the channels exhibited unstable gating kinetics over time, termed wanderlust kinetics by Silberberg et al. (1996), which could encompass a wide range of P_O and various types of kinetic activity, including gating in different apparent modes (see DISCUSSION). Wanderlust kinetics was observed for both wild-type and chimeric channels, so it was not necessarily associated with chimeric channels. Patches with wanderlust kinetics were excluded from analysis.

The methods used to log-bin the intervals into one dimensional (1-D) dwell-time distributions, fit the distributions with sums of exponentials using maximum likelihood fitting techniques, and determine the number of significant exponential components with the likelihood ratio test have been described previously (McManus and Magleby, 1988, 1991; Colquhoun and Sigworth, 1995). Dwell-time distributions are plotted with the Sigworth and Sine (1987) transformation, which plots the square root of the number of intervals per bin without correcting for the logarithmic increase in bin width with time. With this transform, the peaks in the plots fall at the time constants of the major exponential components.

The method of defining a critical gap (closed interval) to define bursts is detailed in Magleby and Pallotta (1983a). In brief, the 1-D distributions of closed interval durations were first fitted with, typically, the sum of five or six exponential components.

The closed intervals from the one to two exponential components with the longest time constants were then defined as gaps between bursts. There was usually a difference of one to three orders of magnitude in the time constants separating the components generating gaps between bursts from those generating closed intervals within bursts, so that the designation of the components was clear. A critical time was then defined to separate closed intervals that were gaps between bursts from those that were gaps within bursts, so that the numbers of misclassified closed intervals would cancel out.

For all mSlo1 tail channels and mSlo3 tail channels, burst analysis was performed on data from patches containing a single channel in which the $P_O < 0.75$, as it became increasingly difficult to define gaps between bursts as P_O increased above this value. For mSlo1 and mSlo3 wild-type channels, burst analysis was performed on single-channel patches and also on some multichannel patches when the channel activity was sufficiently low so that only one channel was open at a time. In these patches, the open probability was calculated by dividing the total open time by the total record length, and then by the number of channels in the patch. The mean durations of the gaps between bursts were estimated in multichannel patches by determining the mean gap between bursts as if the data were from a single channel, and then multiplying the mean durations of the gaps by the numbers of channels in the patch. There was no need to correct estimates of the mean burst duration, mean open time, or mean number of openings per burst, since only one channel was open at any given time during a burst.

Two dimensional (2-D) dwell-time distributions were generated as detailed in Rothberg and Magleby (1998a) and plotted by extending the Sigworth and Sine (1987) transformation to two dwell-time distributions. Briefly, every open interval and its following (adjacent) closed interval were binned as well as every closed interval and its following (adjacent) open interval, with the logs of the open and closed interval durations of each pair locating the bin on the y- and x-axes, respectively.

Dependency plots were constructed from the 2-D dwell-time distributions as described in Magleby and Song (1992). The dependency for each bin of open-closed interval pairs with mean durations t_o and t_c is:

$$Dependency(t_o,t_c) = \frac{N_{obs}(t_o,t_c) - N_{ind}(t_o,t_c)}{N_{ind}(t_o,t_c)}, \quad (1)$$

where $N_{obs}(t_o,t_c)$ is the observed number of interval pairs in bin (t_o,t_c), and $N_{ind}(t_o,t_c)$ is the calculated number of interval pairs in bin (t_o,t_c) if adjacent open and closed intervals pair independently (at random). The expected number of interval pairs in bin (t_o,t_c) for independent pairing is:

$$N_{ind}(t_o,t_c) = P(t_o) \times P(t_c), \quad (2)$$

where $P(t_o)$ is the probability of an open interval falling in the row of bins with a mean open duration of t_o, and $P(t_c)$ is the probability of a closed interval falling in the column of bins with a mean closed duration of t_c. $P(t_o)$ is given by the number of open intervals in row t_o divided by the total number of open intervals, and $P(t_c)$ is given by the number of closed intervals in column t_c divided by the total number of closed intervals.

Single-channel current amplitudes were obtained by plotting histograms of the number of observations versus current amplitude and then measuring the distance between the peaks, which represents the closed and open current levels, and also by visually fitting cursor lines to closed and open single-channel current levels in displayed current records. Similar results were obtained using both methods.

For the TEA experiments, the concentrations of TEA_i that reduced the single-channel current amplitude by 50% (K_d) at membrane potentials ranging from +30 to +90 mV were estimated from fits of a Langmuir function to plots of percent current versus TEA_i. The fraction of current remaining, $1 - y$, is:

$$1 - y = 1/(1 + TEA_I/K_d). \quad (3)$$

K_d values at 0 mV were estimated using the Woodhull (1973) equation, where the ratio of the single-channel conductance in the absence (g_o) and presence (g_B) of blocker at the intracellular side of the channel is given by:

$$g_o/g_B = 1 + B_i[\exp(zd\mathrm{VF}/\mathrm{RT})]/K_d(0\ \mathrm{mv}), \quad (4)$$

where z, B_i, K_d (0 mV) are the blocker valence, concentration, and zero-voltage dissociation constant, respectively, and d is the fraction of voltage drop at the blocking site measured from the intracellular side of the membrane (Coronado and Miller, 1982; Blatz and Magleby, 1984). When Eq. 4 is linearized by taking the natural log of each side, the slope of a plot of $\ln[(g_O/g_B) - 1]$ versus membrane potential equals zdF/RT. Thus, d = slope(RT/Fz), and K_d (0 mV) = B_i/exp(y-intercept).

Statistics

Results are presented as the mean ± SEM. Unless otherwise indicated, differences among group means were tested for significance using the *t* test.

RESULTS

Fig. 1 presents a schematic diagram of the wild-type and chimeric channels studied in this paper to investigate the contribution of the tail domain of BK channels to the gating and conductance properties of the channel. The proposed membrane topology of the Slo family of channels consists of seven transmembrane segments S0–S6 plus a pore (P)-forming region, together with four hydrophobic intracellular regions S7–S10 (Meera et al., 1997; Schreiber et al., 1998, 1999). The calcium bowl in the tail of mSlo1, a highly Ca^{2+}-sensitive BK channel cloned from mouse brain, has eight negative charges and has been implicated in the sensing of Ca^{2+} (Schreiber and Salkoff, 1997; Schreiber et al., 1999). In contrast, the region of the calcium bowl in the tail of mSlo3, a Ca^{2+}-insensitive channel from spermatocytes, contains only two negative charges and provides little, if any, Ca^{2+} sensitivity (Schreiber et al., 1999). Wild-type mSlo1 and mSlo3 channels can be divided into separate core (S0–S8) and tail (S9–S10) regions by removal of a section of the unconserved linker between S8 and S9 (Wei et al., 1994; Schreiber et al., 1999). The core regions of these two different Slo channels have ~56% identity and the tail regions have ~38% identity. As detailed in Fig. 1, our paper studies wild-type mSlo1, wild-type mSlo3, a chimera expressed from the core of mSlo1 plus the tail of mSlo1 (mSlo1 tail channels), and a chimera expressed from the core of mSlo1 plus the tail of mSlo3 (mSlo3 tail channels).

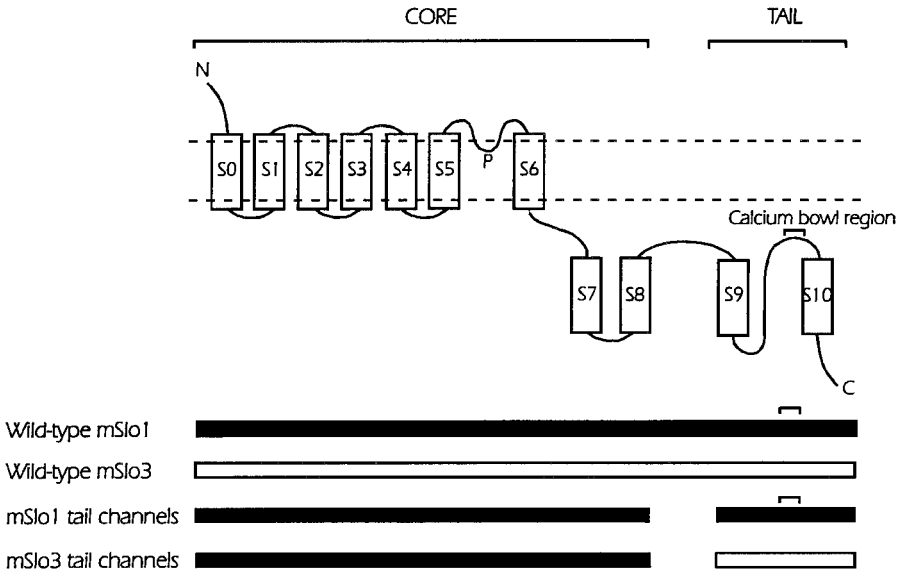

FIGURE 1. Schematic diagram of wild-type mSlo1 channels, wild-type mSlo3 channels, mSlo1 tail channels and mSlo3 tail channels. The position of the calcium bowl in the mSlo1 tail is indicated. The proposed membrane topology of the four studied channels is shown in the top diagram and the components of the various channels is indicated in the schematic diagrams below. The mSlo1 tail channels are expressed from mSlo1 core domains (S0–S8) and mSlo1 tail domains (S9–S10). The mSlo3 tail channels are expressed from mSlo1core domains and mSlo3 tail domains. The mSlo3 core domain (residues 35–641) shares 56% identity with the mSlo1 core domain. The mSlo3 tail domain (residues 686–1136) shares 39% identity with the mSlo1 tail domain (Schreiber et al., 1998). A linker region with little identity is found between S8 and S9. Compared with the mSlo1 tail, the mSlo3 tail has six fewer negatively charged residues in the calcium bowl region. (Adapted from Schreiber et al., 1999.)

Functional channels are not expressed from the core of mSlo3 and the tail of mSlo1 (Schreiber et al., 1999).

Comparison of Kinetic Properties between Wild-type mSlo1 and Wild-type mSlo3

Fig. 2 presents single-channel currents recorded from mSlo1 and mSlo3. In later sections of this paper, we study a chimera made from the core domain (S0–S8) of mSlo1 and the tail domain (S9–S10) of mSlo3 to examine the contribution of the tail domain to the gating. To interpret the chimeric data, it is first necessary to know how the properties of the two wild-type channel types differ. Some of the differences have already been characterized by Schreiber et al. (1998). They found that mSlo3 channels are Ca^{2+}-insensitive in contrast to the high characteristic Ca^{2+} sensitivity of mSlo1 and all other BK channels. They also found that the voltage sensitivity of mSlo3 channels ($\sim$16 mV/e-fold change in P_O) was similar to the voltage sensitivity of mSlo1 (Butler et al., 1993; Cui et al., 1997), and that the conductance of mSlo3 channels ($\sim$106 pS) was considerably less than that of mSlo1 channels ($\sim$270 pS; Butler et al., 1993). In addition, they observed that mSlo3 channels have very brief open times, suggesting that the gating kinetics of mSlo3 also differ from mSlo1.

To characterize the difference in gating kinetics between mSlo3 and mSlo1, an experimental condition was found that gave similar P_O's for the two channels so that the kinetics could be compared. Comparison at similar P_O's is necessary, as the mean open times and burst duration of BK channels such as mSlo1 change with P_O (Magleby and Pallotta, 1983a,b; Nimigean and Magleby, 1999, 2000). As shown in Fig. 2 A for single-channel currents obtained at $\sim$0 μM Ca^{2+}_i and +80 mV, mSlo3 ($P_O \sim 0.05$) had much briefer open times, shorter burst durations, and a lower single-channel conductance than mSlo1 ($P_O \sim 0.04$). These differences are readily apparent in Fig. 2 B, which shows the currents on a faster time base.

To quantify the difference in bursting kinetics between these two channel types, we measured mean burst duration, mean open time, mean number of openings per burst, and the mean duration of the gaps (closed intervals) between bursts. Bursts were identified by using 1-D closed dwell-time distributions to define a critical gap. Closed intervals longer than the critical gap were then taken as gaps between bursts (MATERIALS AND METHODS). Fig. 2 (D and F) presents the 1-D closed dwell-time distributions for the channels presented in Fig. 2, A and B. The arrows indicate the mean gap durations. The dashed line in Fig. 2 D indicates the distribution of effective gap durations after correcting for the three channels in the patch (MATERIALS AND METHODS). For these two experiments, the mean burst duration of mSlo3 (0.42 ms) was approximately sevenfold briefer than that of mSlo1 (2.8 ms). The briefer burst duration of the mSlo3 channel was largely due to the approximately sixfold decrease in mean open time of 0.55 ms for mSlo1 to 0.09 ms for mSlo3. The difference in mean open times can be seen by comparing the open dwell-time distributions in Fig. 2 (C and E), where the mean open times are indicated by arrows. In spite of the

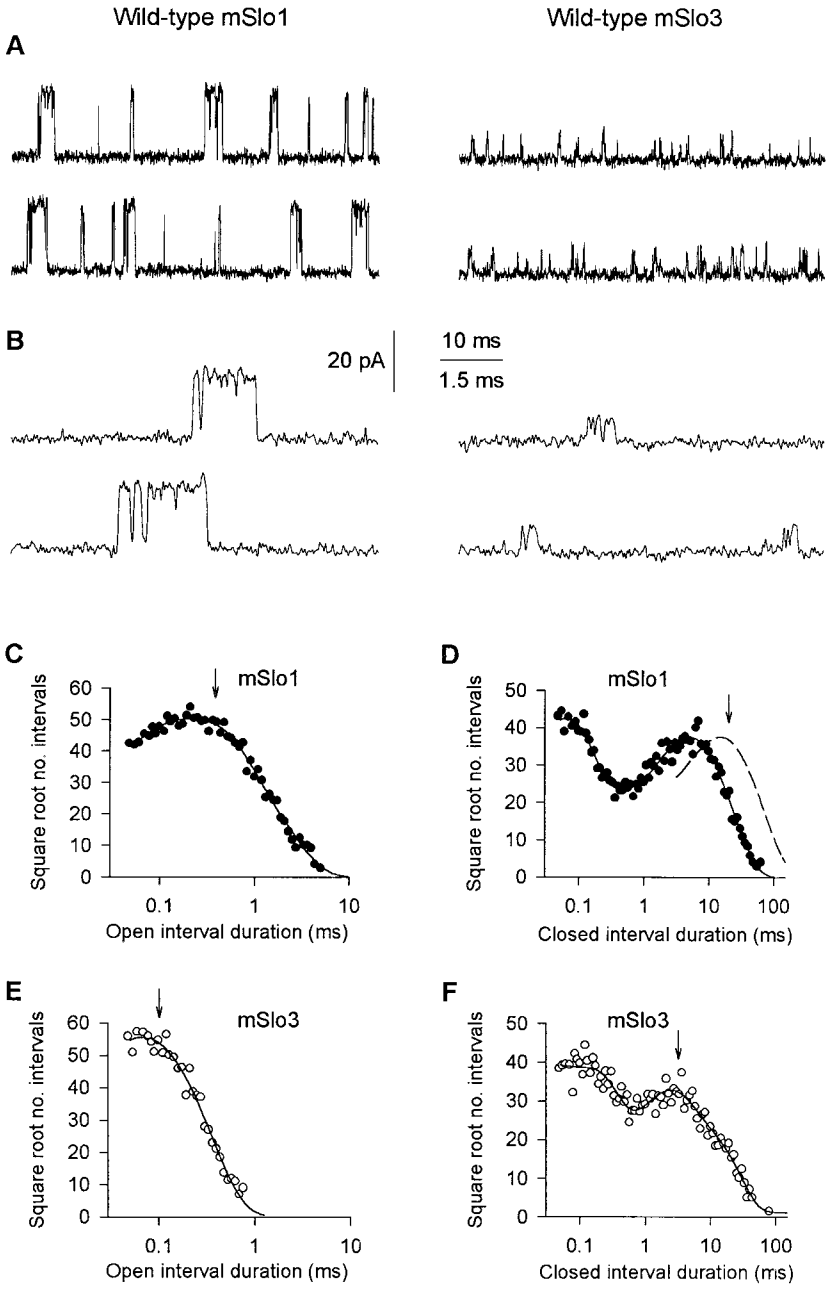

FIGURE 2. Wild-type mSlo1 channels and wild-type mSlo3 channels have different single-channel kinetics. (A) Single-channel current recordings from wild-type mSlo1 and wild-type mSlo3. Upward (outward) currents indicate channel opening. The mSlo1 patch contained three channels, with a mean P_O = 0.040. The mSlo3 patch contained a single channel with a P_O = 0.047. $Ca^{2+}{}_i$ = 0 μM, pH 7.4. Membrane potential = +80 mV. Currents were low-pass filtered at 8 kHz. (B) Representative bursts of openings from A on a faster time base. (C–F) Open and closed 1-D dwell-time distributions for mSlo1 (C and D) and mSlo3 (E and F). The distributions have been scaled to contain the same number of intervals (100,000) to facilitate comparison. The dashed line in D indicates the duration of gaps between bursts after correcting for the number of channels in the patch (MATERIALS AND METHODS). The arrows indicate the mean open times and mean durations of the gaps between bursts. The continuous lines are fits with sums of exponential components with the following time constants and areas. (C, open) 0.07 ms, 0.26; 0.28 ms, 0.54; 0.73 ms, 0.20. (D, closed) 0.06 ms, 0.46; 0.21 ms, 0.09; 3.30 ms, 0.17; 7.22 ms, 0.28. (E, open) 0.04 ms, 0.34; 0.10 ms, 0.66. (F, closed) 0.02 ms, 0.25; 0.14 ms, 0.38; 1.93 ms, 0.23; 7.58 ms, 0.14.

briefer burst duration for mSlo3, the P_O's for the two channels were similar because the mean gap duration for mSlo3 (4.2 ms) was approximately sixfold briefer than the mean gap duration for mSlo1 (24.2 ms).

Burst parameters from experiments such as those shown in Fig. 2 were obtained from a total of five patches with mSlo1 (P_O range: 0.01–0.04) and five patches with mSlo3 (P_O range: 0.01–0.05). Results are summarized in Fig. 3. Mean burst duration, mean open time, and the mean duration of gaps between bursts were ~4-fold, ~3-fold, and ~2.3-fold less, respectively, for mSlo3 than for mSlo1. There was no significant difference in the mean numbers of openings per burst. In these same experiments, the single-channel conductance was 100 ± 4 pS for mSlo3 and 271 ± 4 pS for mSlo1, which is consistent with values reported previously for these channels (Butler et al., 1993; Schreiber et al., 1998). The remainder of this paper will examine to what extent the tail domain of the channels contributes to the functional differences between mSlo1 and mSlo3.

Replacing the mSlo1 Tail with the mSlo3 Tail Greatly Decreases Ca^{2+} Sensitivity and Increases Open Probability in the Absence of Ca^{2+}

To examine the effect of replacing the mSlo1 tail with the mSlo3 tail on the Ca^{2+} sensitivity of P_O and on the

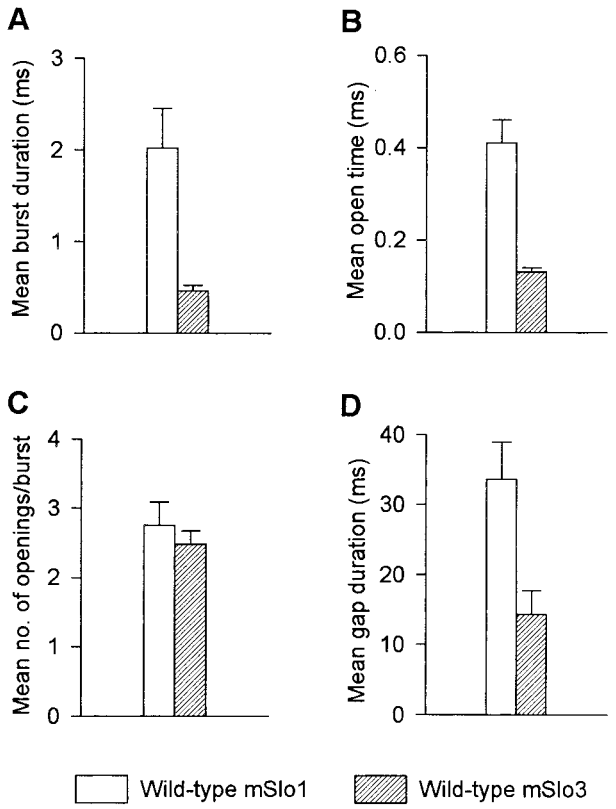

FIGURE 3. Bursting kinetics for wild-type mSlo1 channels differ from wild-type mSlo3 channels at comparable P_O's. (A–D) Plots of the indicated mean bursting parameters for each channel type. Compared with mSlo1 channels, mSlo3 channels showed a briefer mean burst duration ($P < 0.01$), a briefer mean open time ($P < 0.001$), and a briefer mean gap duration between bursts ($P < 0.02$), while showing no significant difference in the mean number of openings per burst ($P = 0.5$). Error bars represent SEM. Data were obtained from five patches containing mSlo1 channels and five patches containing mSlo3 channels. Mean P_O: mSlo1 = 0.030 ± 0.005 (range: 0.014–0.040); mSlo3 = 0.030 ± 0.009 (range: 0.011–0.055). All data were obtained at a Ca^{2+}_i of 0 μM and a membrane potential of +80 mV.

basal activity in the absence of Ca^{2+}_i, single-channel currents were recorded from channels comprised of the mSlo1 core domain and either the mSlo1 tail domain (mSlo1 tail channels) or the mSlo3 tail domain (mSlo3 tail channels), as diagramed in Fig. 1. Fig. 4 A presents currents recorded at +30 mV with 0, 8.7, and 67 μM Ca^{2+}_i from a single mSlo1 tail channel and from a single mSlo3 tail channel. Three observations are immediately apparent from these current records: (1) the level of activity in 0 Ca^{2+}_i was higher for the mSlo3 tail channel than for the mSlo1 tail channel; (2) the effect of Ca^{2+}_i on increasing P_O (Ca^{2+} sensitivity) was far less for the mSlo3 tail channel than for the mSlo1 tail channel; and (3) the high Ca^{2+}_i (67 μM) only drove the P_O of the mSlo3 tail channel to ~0.2 compared with almost complete activation for the mSlo1 tail channel.

To examine further this marked difference in Ca^{2+} sensitivity, P_O was plotted against Ca^{2+}_i for four mSlo1 tail channels in Fig. 4 B and seven mSlo3 tail channels in Fig. 4 C (+30 mV). Unlike the mSlo1 tail channels that all had a very low P_O in the absence of Ca^{2+}_i (0.0005 ± 0.0003), four of the mSlo3 tail channels showed a relatively high level of activity in the absence of Ca^{2+}_i, with P_O's ranging from 0.14 to 0.34, and three showed lower P_O's, ranging from 0.0001 to 0.01. (The reason for the wide range in activity for mSlo3 tail channels in the absence of Ca^{2+}_i is not known, but a wide range of activity was observed in two separate series of experiments, and will be addressed in the DISCUSSION.) Also, unlike the mSlo1 tail channels, which had P_O's approaching 0.96 at 67 μM Ca^{2+}_i, the mSlo3 tail channels were not fully activated at +30 mV, even with 1,000 μM Ca^{2+}_i, where the mean P_O was 0.43 ± 0.08. This lack of maximal activation is not because mSlo3 tail channels have reached some type of inherent limit, as depolarization of mSlo3 tail channels can drive them to high levels of activity (see Fig. 6).

All four mSlo1 tail channels showed a steep increase in P_O with increasing Ca^{2+}_i (Fig. 4 B). The mean Hill coefficient was 3.2 ± 0.2 (range: 2.9–3.5) and the mean Ca^{2+}_i required to achieve a P_O of 0.5 (K_d) was 11.8 ± 1.5 μM (range: 8.3–14.2). These results are within the range of previous observations for wild-type mSlo1 (Butler et al., 1993; Cui et al., 1997; Nimigean and Magleby, 1999).

In contrast to the high Ca^{2+} sensitivity of the mSlo1 tail channels, the mSlo3 tail channels showed a much smaller increase in P_O with increasing Ca^{2+}_i. Accurate estimates of the Hill coefficients could not be obtained for the mSlo3 tail channel because, except for one channel that appeared to reach a maximum P_O, it was unclear whether maximum activation was reached for the other channels, even with 1,000 μM Ca^{2+}_i. Higher concentrations than this were not examined because of the possibility of effects of Ca^{2+}_i on low affinity Mg^{2+} sites (Golowasch et al., 1986; Solaro et al., 1995; Shi and Cui, 2001). Consequently, estimates of the upper limits of the Hill coefficients for mSlo3 tail channels were obtained by setting the maximum level of P_O to the maximum level of P_O typically observed in these experiments (0.5), and estimates for the lower limit were obtained by setting the maximum level of P_O to 0.96, the highest channel activity typically observed under any conditions. The upper limit on the estimated mean Hill coefficient for the mSlo3 tail channels was 1.3 ± 0.5 (range: 0.7–2.0), and the lower limit was 0.55 ± 0.2 (range: 0.05–1.4). These estimates were ~20–45% of those for the mSlo1 tail channels, and only apply over a limited range of P_O. The K_ds for the mSlo3 tail channels were 13, 34, 140, 340, 500, 700, and 9,200 μM when the maximum P_O was set to 0.5, and were 440, 740, 1,200, 1,500, 24,000, and 29,000 μM when the maximum P_O was set to 0.96. The

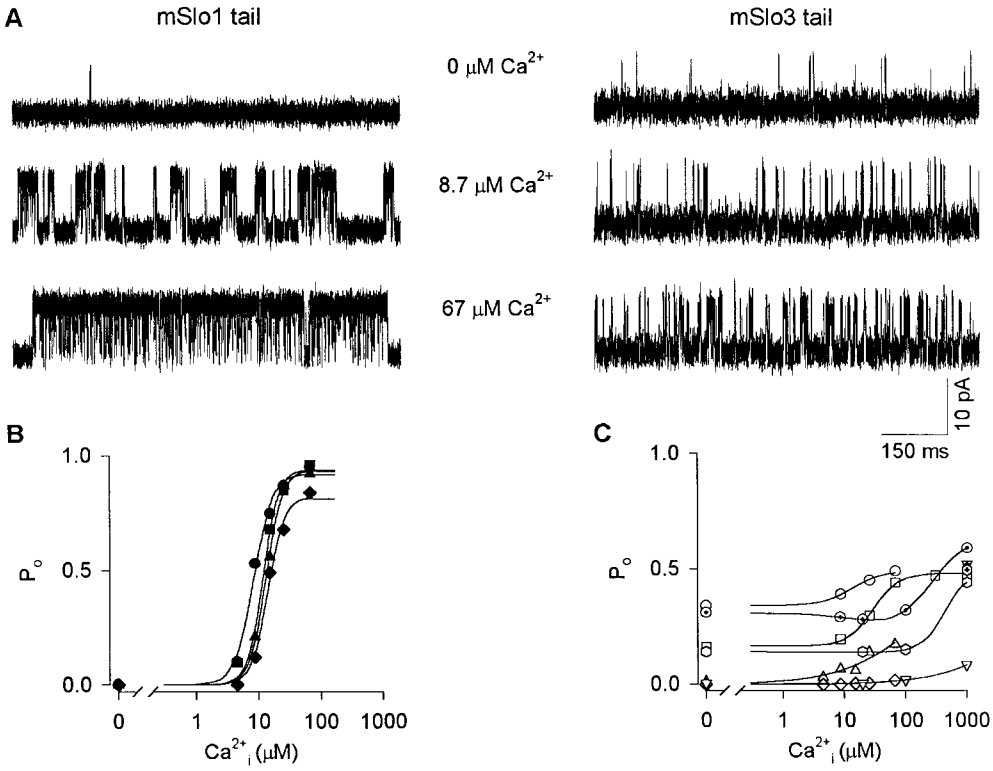

FIGURE 4. Replacing the mSlo1 tail with the mSlo3 tail greatly decreases Ca^{2+} sensitivity and increases activity in the absence of Ca^{2+}. (A) Single-channel currents recorded from a single mSlo1 tail channel and a single mSlo3 tail channel at different Ca^{2+}_i. Membrane potential: +30 mV. Currents were low-pass filtered at 8 kHz. (B and C) Plots of P_O versus Ca^{2+}_i for four mSlo1 tail channels (B) and seven mSlo3 tail channels (C). The lines are fits of the Hill equation, with the mean values of the parameters given in the text. The mSlo1 tail and mSlo3 tail channels in A are represented by closed and open triangles, respectively, in B and C.

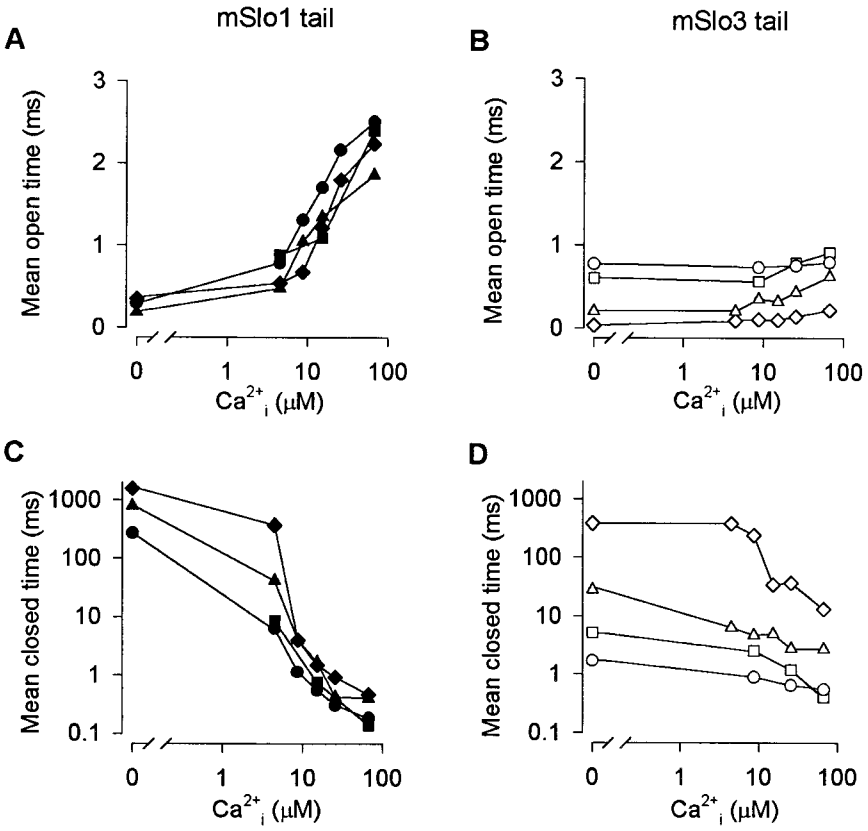

FIGURE 5. Replacing the mSlo1 tail with the mSlo3 tail decreases the Ca^{2+} sensitivity of both mean open and mean closed times. Mean open time and mean closed time versus Ca^{2+}_i for four mSlo1 tail channels (A and C) and four mSlo3 tail channels (B and D). Symbols correspond to those in Fig. 4. Membrane potential: +30 mV. Currents were low-pass filtered at 8 kHz.

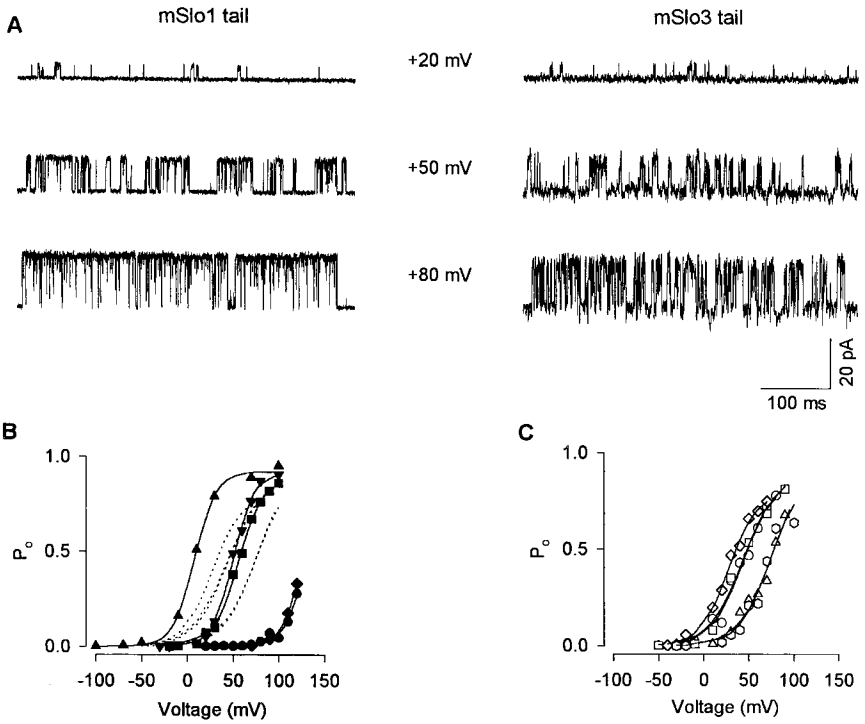

Figure 6. Replacing the mSlo1 tail with the mSlo3 tail decreases the voltage dependence. (A) Single-channel recordings from patches containing a single mSlo1 tail channel and a single mSlo3 tail channel at the indicated membrane potentials. The records were low-pass filtered at 3 kHz. (B and C) Plots of P_O versus membrane potential for five mSlo1 tail channels (B) and five mSlo3 tail channels (C). The lines are fits of the Boltzmann equation, with the mean values of the parameters given in the text. For ease of comparison, the dotted lines in B plot the fits to the mSlo3 tail channels in C. The mSlo1 tail channels were studied in 0 μM (closed circle, closed diamond), 8.7 μM (closed inverted triangle and closed square) and 25.6 μM (closed triangle) $Ca^{2+}{}_i$. The mSlo3 tail channels were studied in 0 μM (open triangle, open square, and open circle), 8.7 μM (open diamond), and 15.2 μM (open hexagon) $Ca^{2+}{}_i$. The records shown in A are represented by inverted closed triangles in B for the mSlo1 tail channel and by upright open triangles in C for the mSlo3 tail channel.

wide variability in the estimated K_ds indicates that some unknown factor is not under control, but in any case, the K_ds for mSlo3 tail channels are typically considerably greater than for mSlo1 tail channels.

Since the activity of wild-type mSlo3 channels is pH-dependent, the question arises whether the small effects of $Ca^{2+}{}_i$ might be due to a small but systematic change in the pH of the solutions below the resolution of the pH electrode. This is unlikely to be the case, as the mSlo3 tail channels showed little pH sensitivity in preliminary experiments in which the pH was changed from 6.5 to 8.0 (unpublished data), and Schreiber et al. (1999) found that mSlo3 tail channels were not sensitive to pH in the range of 7.0–8.0 in terms of changes in g_{max} or the voltage for half activation.

Replacing the mSlo1 Tail with the mSlo3 Tail Decreases the Ca^{2+} Dependence of Both Mean Open and Mean Closed Times

To gain insight into the mechanism of the difference in Ca^{2+} sensitivity between mSlo1 tail channels and mSlo3 tail channels, mean open and closed interval durations were measured and plotted versus $Ca^{2+}{}_i$ for the same channels presented in Fig. 4. Increasing $Ca^{2+}{}_i$ from 0 to 67 μM increased the mean open time of mSlo1 tail channels approximately eightfold (Fig. 5 A), with little or no increase in the mean open time of mSlo3 tail channels (Fig. 5 B). Over the same range of $Ca^{2+}{}_i$, the mean closed time of mSlo1 tail channels decreased ~2,300-fold (Fig. 5 C), compared with an ~14-fold decrease in the mean closed time of mSlo3 tail channels (Fig. 5 D). Thus, the greatly decreased Ca^{2+} sensitivity of mSlo3 tail channels reflects a greatly decreased Ca^{2+} dependence of both mean open time and mean closed time.

Replacing the mSlo1 Tail with the mSlo3 Tail Decreases the Voltage Dependence

To examine whether replacing the tail of mSlo1 with the tail of mSlo3 altered the voltage dependence of mSlo1, currents were recorded from a single mSlo1 tail channel and a single mSlo3 tail channel at +20, +50, and +80 mV. As shown in Fig. 6 A, both channels had a low activity at +20 mV ($P_O \sim 0.04$), which then increased dramatically with depolarization, with a suggestion that the increase for the mSlo3 tail channel was less than for the mSlo1 tail channel. To examine the voltage dependence further, we plotted P_O versus membrane potential for five mSlo1 tail channels in Fig. 6 B

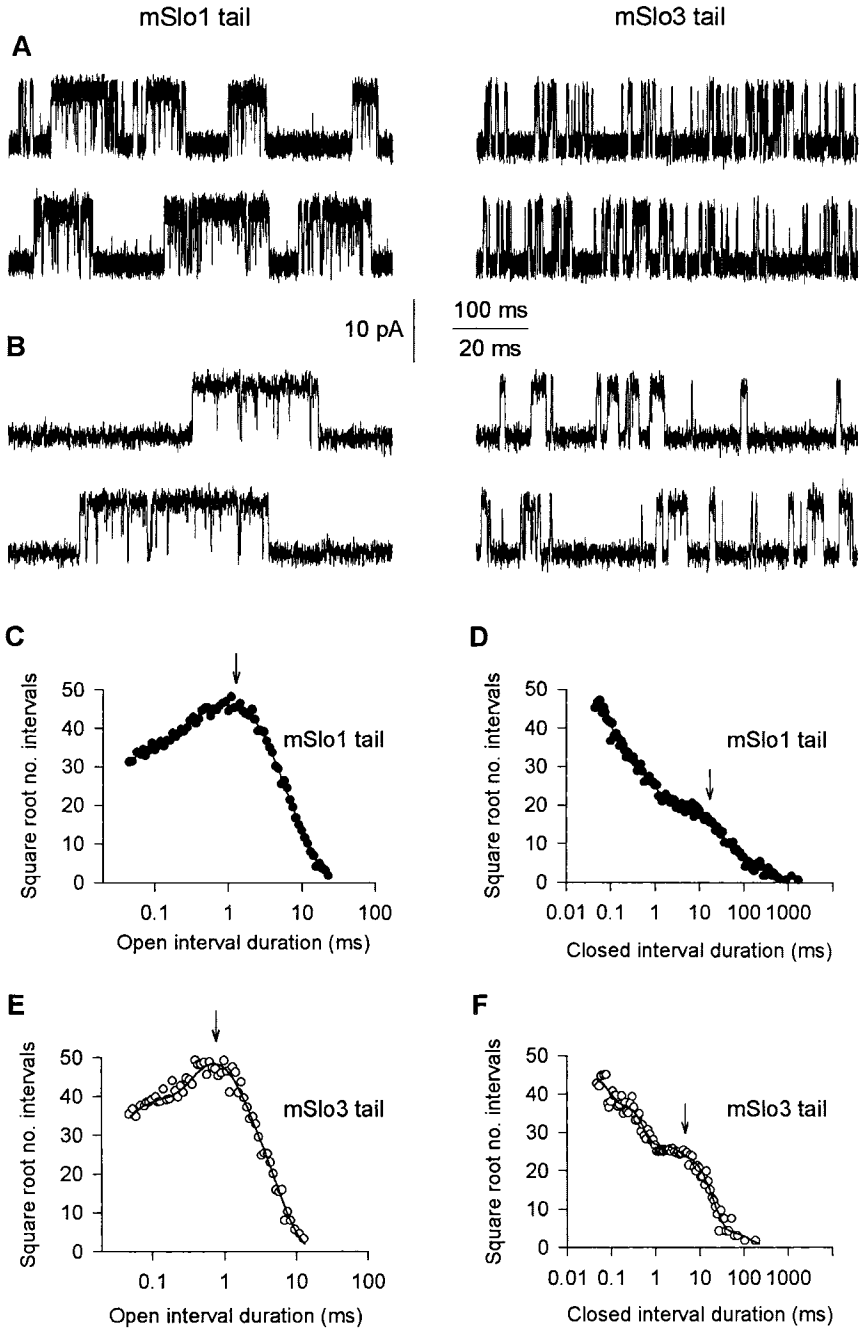

FIGURE 7. Replacing the mSlo1 tail with the mSlo3 tail decreases burst duration. (A) Single-channel current recordings from patches containing a single mSlo1 tail channel and a single mSlo3 tail channel. For the mSlo1 tail channel, Ca^{2+}_i = 15.2 μM and P_O = 0.30. For the mSlo3 tail channel, Ca^{2+}_i = 0 μM and P_O = 0.34. Membrane potential: +30 mV. Both recordings were low-pass filtered at 8 kHz. (B) Representative bursts of openings from A on a faster time base. (C–F) Open and closed 1-D dwell-time distributions for the mSlo1 tail channel (C and D) and mSlo3 tail channel (E and F) shown in A and B. The distributions have been scaled to contain the same number of intervals (100,000) to facilitate comparison. The arrows indicate the mean open times and the mean durations of the gaps between bursts. The time constants and areas of the exponential components are as follows. (C, open) 0.05 ms, 0.16; 0.27 ms, 0.20; 1.08 ms, 0.39; 2.57 ms, 0.25. (D, closed) 0.03 ms, 0.44; 0.11 ms, 0.21; 0.35 ms, 0.15; 1.17 ms, 0.08; 6.15 ms, 0.08; 22.94 ms, 0.04. (E, open) 0.06 ms, 0.23; 0.56 ms, 0.45; 1.49 ms, 0.32. (F, closed) 0.03 ms, 0.40; 0.19 ms, 0.32; 1.10 ms, 0.13; 5.74 ms, 0.15.

and five mSlo3 tail channels in Fig. 6 C. The mSlo1 tail channels were studied in 0 μM (Fig. 6, closed circle and closed diamond), 8.7 μM (Fig. 6, closed inverted triangle and closed square), and 25.6 μM (closed triangle) Ca^{2+}_i. The mSlo3 tail channels were studied in 0 μM (open triangle, open square, and open circle), 8.7 μM (open diamond), and 15.2 μM (open hexagon) Ca^{2+}_i. For these particular experiments with mSlo1, the data obtained from different channels at the same Ca^{2+}_i essentially overlap. For mSlo3 channels, there were no consistent relationship between Po and Ca^{2+}_i.

The lines are Boltzmann fits to the data. Only three of the five fits are readily apparent in Fig. 6 C because of the overlap of fitted curves. To facilitate comparison between the channels, the Boltzmann fits to the mSlo3 tail channels in Fig. 6 C are plotted in Fig. 6 B as dotted lines on the plots from the mSlo1 tail channels. A shallower slope for the mSlo3 tail channels is seen, indicating a decreased voltage dependence for the mSlo3 tail channels (17.3 ± 0.9 mV per e-fold change in P_O; range: 15.8–19.5 mV) compared with the mSlo1 tail channels (12.3 ± 0.3 mV; range: 11.7–13.4 mV), and this difference was significant ($P < 0.001$). The estimated effective gating charge

(in units of electronic charge, e_o) for mSlo3 tail channels was 1.49 ± 0.06 (range: 1.31–1.62), and for mSlo1 tail channels was 2.08 ± 0.05 (range: 1.91–2.18). Both these estimates are within the ranges of values reported for wild-type mSlo1 and also other wild-type BK channels (Butler et al., 1993; Cui et al., 1997; Stefani et al., 1997; Rothberg and Magleby, 2000).

Replacing the mSlo1 Tail with the mSlo3 Tail Decreases Burst Duration

The single-channel currents in Figs. 4 and 6 suggest that, in addition to decreasing both Ca^{2+} sensitivity and voltage dependence, replacing the tails of mSlo1 channels with the tails of mSlo3 channels may also decrease burst duration. To examine this possibility, we compared mSlo1 tail channels and mSlo3 tail channels at similar P_O's, to control for the fact that the burst duration of mSlo1 channels increases with P_O, independent of whether the channels are activated by $Ca^{2+}{}_i$ or depolarization (Nimigean and Magleby, 1999, 2000). As shown in Fig. 7 (A and B), which presents single-channel current records from a single mSlo1 tail channel and a single mSlo3 tail channel on two different time bases, the mSlo3 tail channel does appear to have briefer duration bursts, even though the P_O's of the two channels are similar (P_O's of 0.30 and 0.34, for mSlo1 tail and mSlo3 tail, respectively).

To quantify the difference in bursting kinetics between these two channels, we measured several burst parameters including mean burst duration, mean open time, mean number of openings per burst, and mean duration of the gaps (closed intervals) separating bursts. As in the burst analysis of the wild-type channels, bursts were identified by using 1-D closed dwell-time distributions to define a critical gap to separate bursts. Fig. 7 (D and F) presents the 1-D closed dwell-time distributions, and the arrows indicate the mean gap durations. Burst analysis of the single-channel currents indicated that replacing the mSlo1 tail with the mSlo3 tail decreased burst duration 3.4-fold, from 8.6 ms for the mSlo1 tail channel to 2.5 ms for the mSlo3 tail channel. The decreased burst duration of the mSlo3 tail channel was largely due to a decrease in the mean number of openings per burst, from 6.1 for the mSlo1 tail channel to 2.9 for the mSlo3 tail channel, as well as a decrease in mean open time, from 1.2 ms for the mSlo1 tail channel to 0.79 ms for the mSlo3 tail channel. This 34% decrease in mean open time can be seen by comparing the 1-D open dwell-time distributions in Fig. 7 (C and E), where the arrows indicate mean open time. For the same P_O, replacing the mSlo1 tail with the mSlo3 tail also decreased the mean duration of gaps between bursts fourfold, from 17.4 to 4.3 ms (Fig. 7, D and F, arrows).

To characterize the differences in bursting kinetics between mSlo1 tail channels and mSlo3 tail channels over a range of P_O, bursting parameters were measured and plotted against P_O for 10 datasets from three mSlo1 tail channels and 10 datasets from three mSlo3 tail channels (membrane potential: +30 mV; 0–67 μM

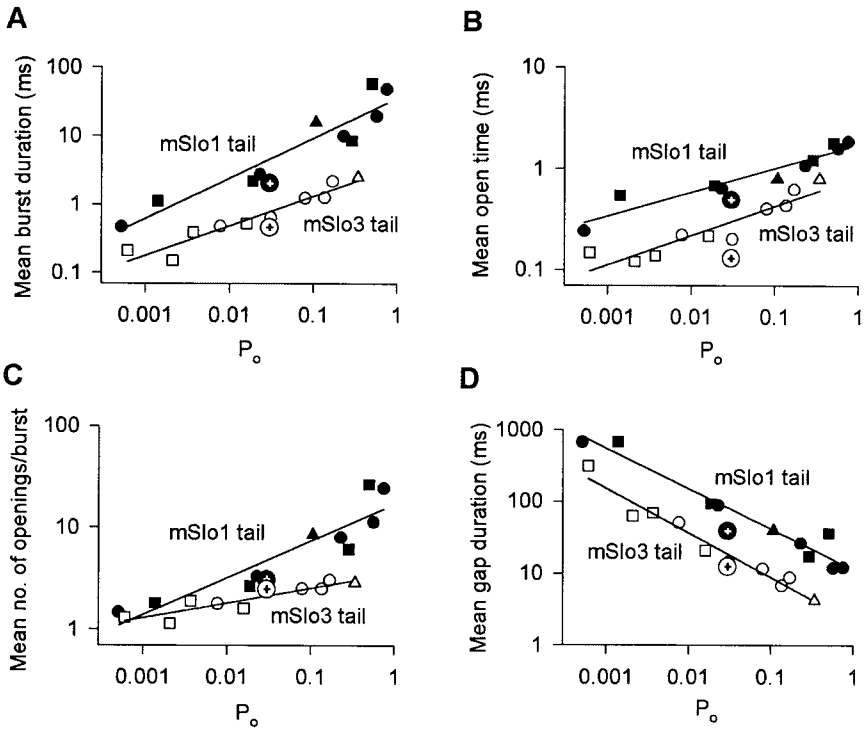

FIGURE 8. Bursting kinetics for mSlo1 tail channels differ from mSlo3 tail channels at the same P_O. (A–D) Plots of indicated bursting parameters versus P_O. Compared with mSlo1 tail channels, mSlo3 tail channels showed a briefer mean burst duration (A), a briefer mean open time (B), a decrease in the mean number of openings per burst (C), and briefer durations of gaps between bursts (D). For both mSlo1 tail channels and mSlo3 tail channels, each plot contains estimates from 10 datasets from three different channels. Membrane potential: +30 mV. All recordings were low-pass filtered at 8 kHz. Each symbol type plots data from a different channel. The channels shown in Fig. 7 (A and B) are represented by a closed square for the mSlo1 tail channel and an open triangle for the mSlo3 tail channel. For comparison, each plot includes the mean burst parameters for the wild-type mSlo1 channels (closed circle with crosshair) and wild-type mSlo3 channels (open circle with crosshair) from Fig. 3.

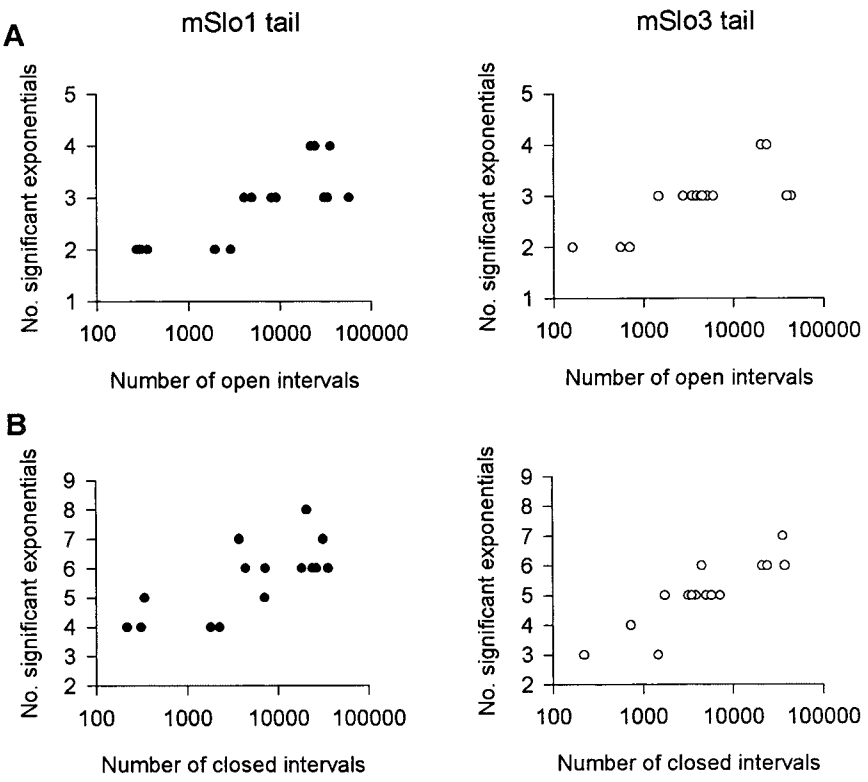

FIGURE 9. Replacing the mSlo1 tail with the mSlo3 tail does not change the number of detected kinetic states entered during gating. Estimates of the number of detected open (A) and closed (B) states entered during gating plotted against the number of intervals analyzed. Estimates plot the number of significant exponential components required to describe the 1-D dwell-time distributions. For each channel type, the 15 estimates of the open states and 15 estimates of the closed states are from fitting 15 different datasets from five different single-channel patches. Multiple datasets were obtained from each channel by obtaining data at different Ca^{2+}_i, which ranged from 0 to 67 μM. Membrane potential: +30 mV. All recordings were low-pass filtered at 8 kHz.

Ca^{2+}_i). As shown in Fig. 8 A, the mean burst duration of mSlo3 tail channels was three- to ninefold briefer than that of mSlo1 tail channels over the range of P_O examined (0.0005–0.75). The briefer burst duration was associated with a two- to threefold decrease in mean open time (Fig. 8 B) and a decrease in the mean number of openings per burst (Fig. 8 C). In addition, the gaps between bursts for the mSlo3 tail channels were four- to fivefold briefer than those for mSlo1 tail channels (Fig. 8 D). Thus, replacing the mSlo1 tail with the mSlo3 tail resulted in a consistent and pronounced modulation of bursting kinetics over an ~1,500-fold range of P_O.

If the tail domain of the Slo family of channels modulates the bursting kinetics, then it might be expected that transferring the tail of mSlo3 to mSlo1 would also transfer the bursting kinetic properties of mSlo3. To test this hypothesis, the parameters defining the bursting kinetics of wild-type mSlo1 and wild-type mSlo3 channels are plotted on Fig. 8 (large circles containing a plus sign) for comparison to the kinetics of mSlo1 tail channels and mSlo3 tail channels. In general, replacing the tail of mSlo1 with the tail of mSlo3 transferred the bursting kinetic properties of wild-type mSlo3 channels.

Replacing the mSlo1 Tail with the mSlo3 Tail Does Not Change the Number of Detected Kinetic States Entered during Gating

BK channel gating has been well-described by schemes in which the channel enters multiple kinetically distinct open and closed states (McManus and Magleby, 1991; Wu et al., 1995; Cui et al., 1997; Horrigan et al., 1999; Rothberg and Magleby, 1999, 2000; Cui and Aldrich, 2000). Thus, it is possible that the difference in bursting kinetics between mSlo1 tail channels and mSlo3 tail channels may reflect a difference in the number of states each channel enters during gating. The minimum number of open and closed states can be estimated from the number of significant exponential components required to describe dwell-time distributions of open and closed intervals (Colquhoun and Hawkes, 1995). Therefore, we estimated the number of significant exponential components required to fit open and closed 1-D dwell-time distributions for both mSlo1 tail channels and mSlo3 tail channels.

Fig. 9 (A and B) plots estimates of the number of significant exponential components (number of detected states) required to describe the open (A) and closed (B) 1-D dwell-time distributions for 15 datasets from five patches, each containing a single mSlo1 tail channel, and for 15 datasets from five patches, each containing a single mSlo3 tail channel. Multiple datasets were obtained from each channel by obtaining data at different Ca^{2+}_i. The estimates are plotted against the number of intervals analyzed, since the ability to resolve exponential components increases with increasing numbers of intervals (McManus and Magleby, 1988).

Estimates of the minimum number of open states ranged from two to four for both types of channels.

The mean number of detected open states for mSlo1 tail channels (2.9 ± 0.2) was not significantly different ($P < 0.05$, Mann-Whitney test) from the mean number of detected open states for mSlo3 tail channels (2.9 ± 0.2). Estimates of the number of detected closed states ranged from four to eight for mSlo1 tail channels and from three to seven for mSlo3 tail channels. The mean number of detected closed states for mSlo1 tail channels (5.6 ± 0.3) was not significantly different ($P < 0.05$, Mann-Whitney test) from the mean number of detected closed states for mSlo3 tail channels (5.1 ± 0.3). Thus, each channel type typically entered a minimum of three or more open and five to six closed kinetic states during normal activity.

These results suggest that the pronounced difference in bursting kinetics between mSlo1 tail channels and mSlo3 tail channels does not reflect a major difference in the number of detected kinetic states entered during gating. However, we cannot rule out the possibility that mSlo1 tail channels and mSlo3 tail channels do differ in the number of kinetic states entered during gating and that these differences were not detected due to overlapping time constants and/or small areas of some of the exponential components.

mSlo1 Tail Channels and mSlo3 Tail Channels Have Similar Kinetic Structures

Replacing the mSlo1 tail with the mSlo3 tail resulted in a pronounced change in bursting kinetics. Such differences in kinetics could arise from a fundamental change in the gating mechanism or a change in the transition rates among states. The observation that the numbers of detected states did not change would argue against a fundamental change in the gating mechanism, but this is not clear. One way to help distinguish between these two possibilities is to examine the effective connections (transition pathways) among the various open and closed states. 2-D dwell-time distributions, which plot the relative number of occurrences (frequency) various pairs of adjacent open and closed intervals of specified durations are observed in the single-channel record, contain correlation information that can help define these connections (Fredkin et al., 1985; Keller et al., 1990; Magleby and Song, 1992).

Fig. 10 (A and C) presents the 2-D dwell-time distributions for the mSlo1 tail channel and the mSlo3 tail channel, whose single-channel currents were shown in Fig. 7. The y- and x-axes plot the log of the durations of adjacent open and closed intervals, respectively, and the z axis plots the square root of the number of observations per bin. To facilitate comparison, the P_O's were similar for both channel types (0.30 and 0.34). The general shapes of the plots were similar, but with differences in the relative frequency of the various interval pairs. For example, for both channel types, the components of interval pairs that occurred most frequently were long open intervals adjacent to brief closed intervals (Fig. 10, A and C, position 3). These interval pairs typically give rise to openings separated by brief closings within bursts. A major difference in the two plots is that the mSlo3 tail channel shows a higher frequency of brief open intervals adjacent to brief closed intervals (Fig. 10 C, arrow). These interval pairs would contribute to the briefer mean open time and briefer burst duration of mSlo3 tail channels. Also notice that the long closed intervals of the mSlo3 tail channel are shifted toward briefer durations (positions 2 and 4). This shift reflects the briefer duration of gaps between bursts for mSlo3 tail channels. Fig. 10 (E and G) presents 2-D dwell-time distributions for another pair of channels studied at a lower P_O (0.19 and 0.14), where the relative frequency of brief open intervals is much greater for the mSlo3 tail channel than for the mSlo1 tail channel (arrow and position 2). Thus, as would be expected from their differences in bursting kinetics, mSlo1 tail channels and mSlo3 tail channels have differences in the relative frequencies of interval pairs.

In addition to providing a profile of the relative frequencies of interval pairs, the 2-D dwell-time distributions also contain correlation information which gives information about the connections between different open and closed states (and compound states) of different mean lifetimes (Magleby and Song, 1992). This information is not obvious from visual inspection of the 2-D dwell-time distributions, because the relative heights of individual peaks indicate the relative frequency of occurrence of interval pairs of various durations, and not whether any given interval pair is in excess or deficit over what would be expected from independent (random) pairing of the intervals.

Dependency plots provide a means to display this correlation information (Magleby and Song, 1992). A dependency plot presents the fractional difference between the observed number of adjacent open and closed intervals of indicated durations and the hypothetical number that would be observed if all of the open and closed intervals paired independently (Eqs. 1 and 2). For example, dependencies of +0.5 or −0.5 would indicate 50% more or 50% fewer observed interval pairs, respectively, than expected for independent pairing of open and closed intervals. A positive dependency for an interval pair suggests the presence of effective transition pathways between the open and closed kinetic states (and compound states) that give rise to that pair. Conversely, a negative dependency for a given interval pair suggests a deficit of effective transition pathways between the open and closed kinetic states (and compound states) that give rise to that pair (Magleby and Song, 1992; Rothberg et al., 1997; Roth-

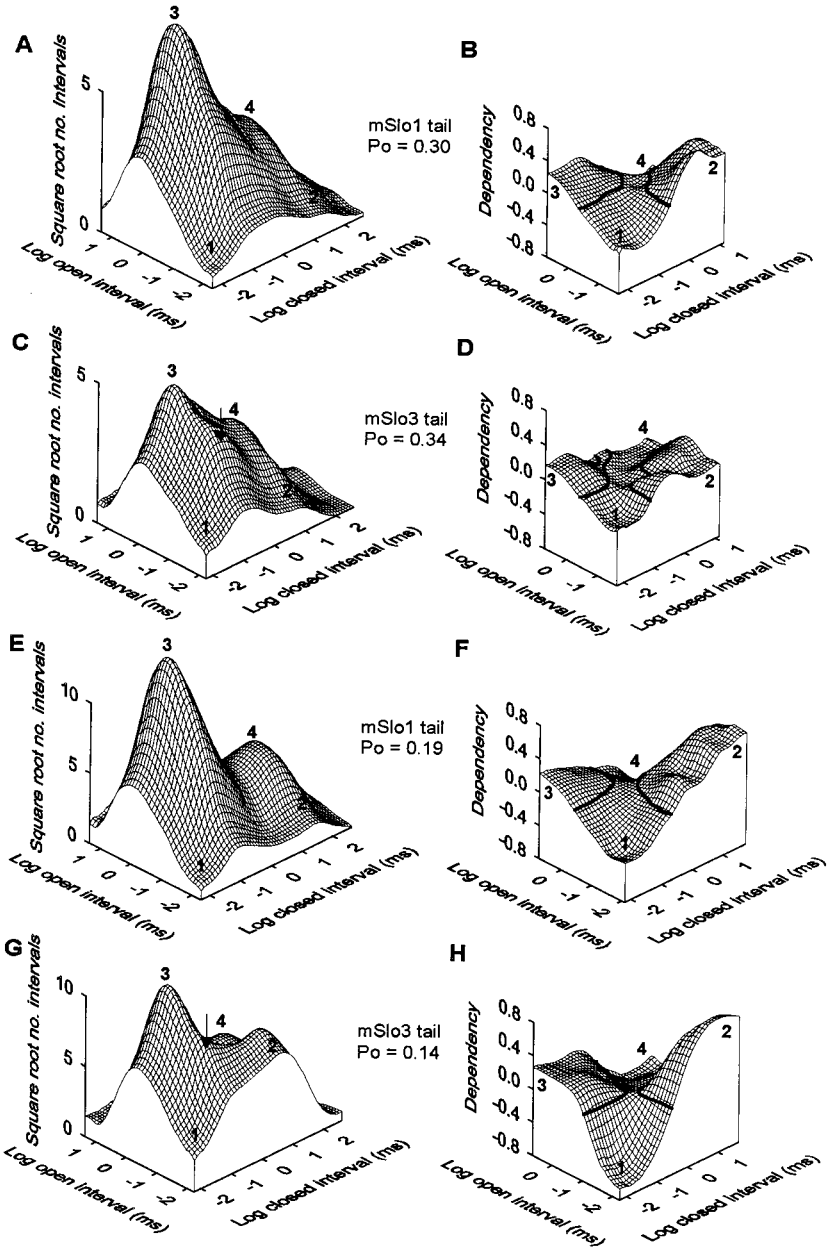

FIGURE 10. A comparison of 2-D dwell-time distributions and dependency plots obtained for mSlo1 tail channels and mSlo3 tail channels at similar P_O's indicates that the two channel types have distinct kinetics, yet similar kinetic structures. Compare A with C and E with G to see differences in the 2-D dwell-time distributions between mSlo1 tail channels and mSlo3 tail channels at comparable P_O's. The arrows in C and G indicate the higher occurrence of brief open intervals adjacent to brief closed intervals observed in mSlo3 tail channels. Compare B with D and F with H to see the similar saddle shape of the dependency plots between mSlo1 tail channels and mSlo3 tail channels. The heavy lines in the dependency plots indicate a dependency of zero. A–D present the 2-D dwell-time distributions and dependency plots for the mSlo1 tail channel and the mSlo3 tail channel shown in Fig. 7.

berg and Magleby, 1998b). Thus, dependency plots reveal the kinetic structure of a channel.

Fig. 10, B and D and F and H, presents dependency plots derived from the 2-D dwell-time distributions in Fig. 10, A and C, and E and G, respectively. Although mSlo1 tail channels and mSlo3 tail channels differ kinetically, a comparison of the four dependency plots suggests that these channels have similar kinetic structures, since the plots for both channel types have the characteristic saddle shape that is typical of dependency plots for BK channels (Rothberg and Magleby, 1998a, 1999). Within the general saddle shape, there is variability in the dependency plots among the channels, but this variability is within the range typically observed for BK channels (Rothberg and Magleby, 1998a, 1999). This variation is considerably less than might be expected for marked differences in the underlying gating mechanism (Magleby and Song, 1992).

The saddle shape in the dependency plots arises from excesses and deficits of specific interval pairs. In particular, plots from both mSlo1 tail channels and mSlo3 tail channels show a deficit of brief open intervals adjacent to brief closed intervals (position 1), an excess of brief open intervals adjacent to long closed intervals (position 2), a deficit of long open intervals adjacent to long closed intervals (position 4), and an excess of long open intervals adjacent to brief closed intervals (position 3).

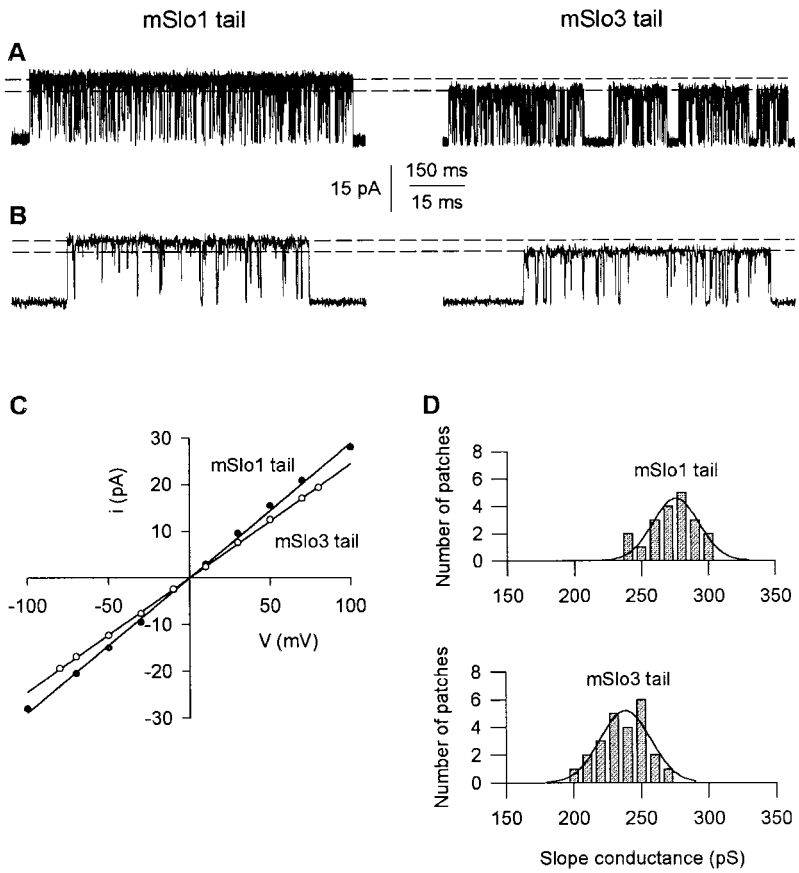

FIGURE 11. Replacing the mSlo1 tail with the mSlo3 tail decreases single-channel conductance. (A) Single-channel current recordings from a single mSlo1 tail channel and a single mSlo3 tail channel. The dashed lines indicate the maximum current amplitude observed for each channel type. Membrane potential: +70 mV. Records were low-pass filtered at 5 kHz. (B) Representative bursts from A on a faster time base. (C) Plots of single-channel current amplitude versus membrane potential for the channels shown in A and B. The slope conductances were 285 pS for the mSlo1 tail channel and 243 pS for the mSlo3 tail channel. (D) Histograms of slope conductance measurements from 20 patches containing mSlo1 tail channels and 24 patches containing mSlo3 tail channels. For each plot, the superimposed line represents the fit of a Gaussian function to the histogram, yielding mean slope conductances of 276 ± 4 pS and 238 ± 4 pS for the mSlo1 tail channels and mSlo3 tail channels, respectively.

Such a saddle-shaped dependency plot indicates that for each channel type, there is a general inverse relationship between the durations of open and closed states and compound states. That is, brief open states (or compound states in each comparison) tend to be adjacent to long closed states, and long open states tend to be adjacent to brief closed states. Thus, the data suggest that the effective connections among the various open and closed states (kinetic structure) are similar between mSlo1 tail channels and mslo3 tail channels, consistent with the idea that the difference in bursting kinetics arises from differences in the transition rates among states rather than from differences in the fundamental gating mechanisms.

Replacing the mSlo1 Tail with the mSlo3 Tail Decreases the Single-channel Conductance

In addition to modulating gating properties, replacing the mSlo1 tail with the mSlo3 tail decreased single-channel conductance. Fig. 11 (A and B) presents single-channel currents recorded from a mSlo1 tail channel and a mSlo3 tail channel at a membrane potential of +70 mV at two different time bases. The dashed lines denote the maximum current amplitude observed for each channel. The mSlo1 tail channel had a maximum amplitude of ~20.9 pA, compared with ~17.3 pA for the mSlo3 tail channel.

To estimate the slope conductances of these two channels, we plotted single-channel current amplitude versus membrane potential. As shown in Fig. 11 C, the difference in current amplitude was observed over a wide range of voltages, with no obvious rectification for either channel. The single-channel conductances were ~285 pS for the mSlo1 tail channel and ~243 pS for the mSlo3 tail channel.

Estimates of slope conductances from plots such as those shown in Fig. 11 C for 20 patches with mSlo1 tail channels and 24 patches with mSlo3 tail channels are presented as histograms in Fig. 11 D. A clear shift toward lower conductances for mSlo3 tail channels was observed. The superimposed lines are fits of Gaussian functions to the distributions, yielding mean slope conductances of 276 ± 4 pS for the mSlo1 tail channels and 238 ± 4 pS for the mSlo3 tail channels. Thus, replacing the mSlo1 tail with the mSlo3 tail results in a 14% reduction in single-channel conductance ($P < 0.001$).

Replacing the mSlo1 Tail with the mSlo3 Tail Increases the Sensitivity to Block by Internal TEA

The lower single-channel conductance observed when the mSlo1 tail is replaced with the mSlo3 tail suggests

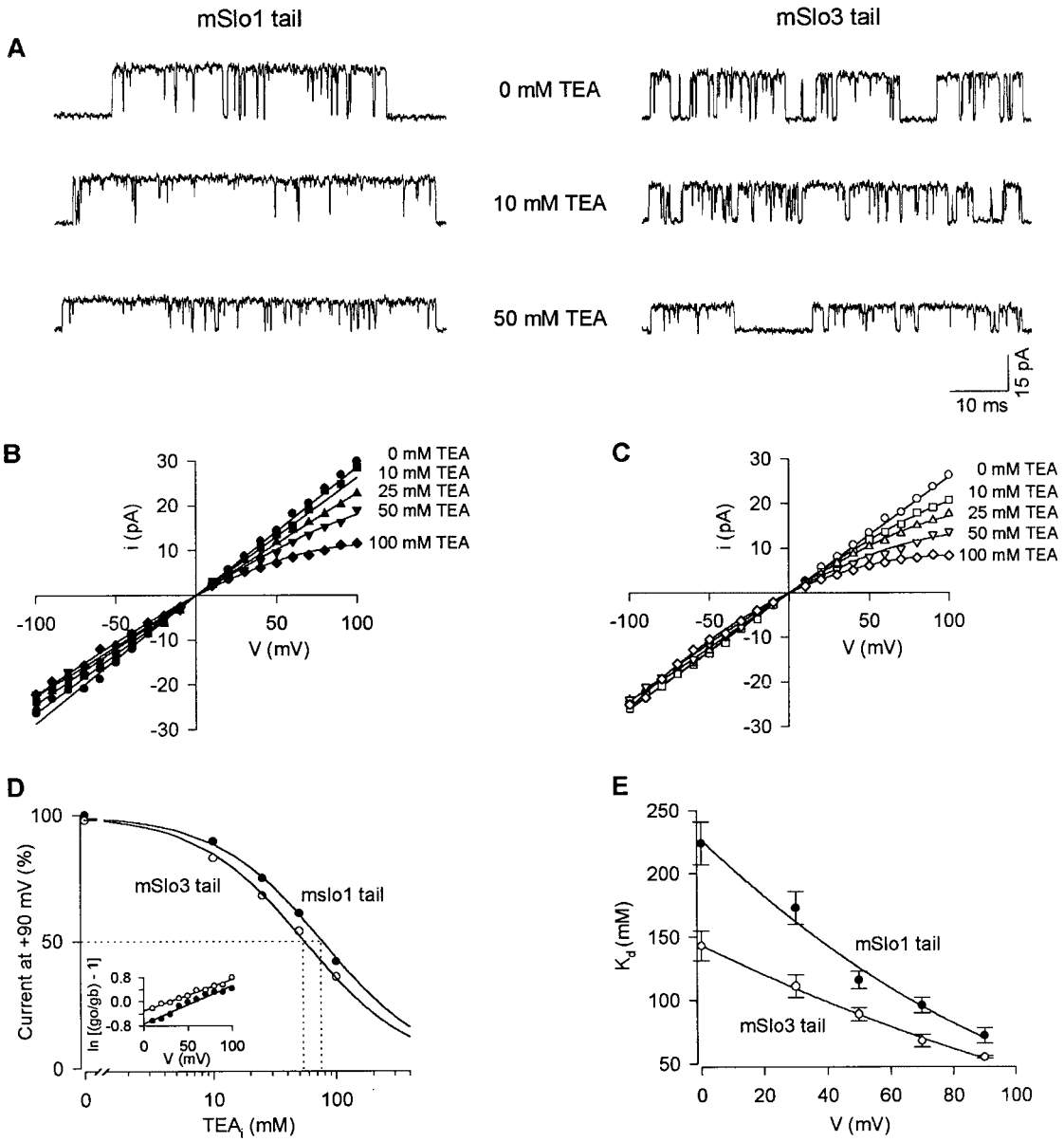

FIGURE 12. Replacing the mSlo1 tail with the mSlo3 tail increases sensitivity to block by internal TEA. (A) Single-channel current recordings from patches containing a single mSlo1 tail channel and a single mSlo3 tail channel at the indicated concentrations of internal TEA (TEA_i). Membrane potential: +70 mV. Recordings were low-pass filtered at 5 kHz. (B and C) Plots of single-channel current amplitude versus membrane potential at the indicated TEA_i for the mSlo1 tail channel (B) and mSlo3 tail channel (C) shown in A. (D) Plot of single-channel current amplitude as a percent maximum current versus TEA_i for the channels shown in A–C, but at a membrane potential of +90 mV. The solid lines are fits of a Langmuir function (Eq. 3) which yielded K_d values (indicated by dotted lines) of 77 mM and 55 mM for the mSlo1 tail channel and mSlo3 tail channel, respectively. K_d values at 0 mV were estimated using the Woodhull (1973) equation (Eq. 4). The inset in D plots $\ln[(g_O/g_B) - 1]$ against membrane potential, where g_O and g_B represent the single-channel conductance in the absence and presence of 100 mM TEA, respectively. Analysis of the y-intercepts yielded K_d values of 207 and 137 mM at 0 mV for the mSlo1 tail channel and mSlo3 tail channel, respectively. (E) Mean K_d (±SEM) values plotted against membrane potential for mSlo1 tail channels (two experiments) and mSlo3 tail channels (three experiments). The lines are regression fits to show the trend in the data.

that the mSlo3 tail alters channel structure or charge distributions in a way that reduces the movement of K^+ through the pore. TEA, which can reduce single-channel conductance of K^+ channels, has been a useful tool for exploring the vestibules of K^+ channels (Armstrong and Hille, 1972; Yellen et al., 1991; Choi et al., 1991; Taglialatela et al., 1993; Slesinger et al., 1993). Therefore, to gain some insight into the change in structure, we compared sensitivity to block by internal TEA when the mSlo1 tail was replaced by the mSlo3 tail.

Fig. 12 A presents current recordings from an mSlo1 tail channel and an mSlo3 tail channel with internal

TEA concentrations (TEA_i) of 0, 10 and 50 mM (+70 mV), showing that TEA reduced the single-channel current amplitude for each channel type. The reduction in current is referred to as a fast block, as discrete blocking events are not observed. Fig. 12 (B and C) plots single-channel current amplitude against membrane potential for the mSlo1 tail channel and mSlo3 tail channel shown in Fig. 12 A. For both channel types, TEA reduced single-channel current amplitude at all potentials examined. The block was voltage-dependent, becoming greater at more positive potentials. Comparison of the degree of block at positive potentials between the two plots suggests that the mSlo3 tail channels are more sensitive to block by internal TEA. For example, at +100 mV, 10 mM TEA reduced the amplitude of currents from the mSlo1 tail channel by ~5% compared with a 20% reduction for the mSlo3 tail channel.

To further characterize this apparent difference in TEA sensitivity, we examined dose–response relationships for each channel type. Fig. 12 D plots the current versus TEA_i for the two channels shown in Fig. 12 (A–C). The solid lines are fits of a Langmuir function (Eq. 3), which yielded K_d values of 77 and 55 mM for the mSlo1 tail channel and mSlo3 tail channel, respectively. The dotted lines in Fig. 12 D show graphically that the K_d for each channel type corresponds to the TEA_i that reduces single-channel current amplitude to 50% of the control value. K_d values were also estimated for data obtained at +30, +50, and +70 mV using the same method, and at 0 mV using the Woodhull (1973) equation (Eq. 4). The inset in Fig. 12 D plots $\ln[(g_O/g_B) - 1]$ against membrane potential, where g_O and g_B represent the single-channel conductance in the absence and presence of 100 mM TEA, respectively. Analysis of the y-intercepts yielded K_d values at 0 mV of 207 and 137 mM for the mSlo1 tail channel and mSlo3 tail channel, respectively. Estimates of K_d values are summarized in Fig. 12 E, which plots mean K_d versus membrane potential for mSlo1 tail channels (two experiments) and mSlo3 tail channels (three experiments). The K_d values for the mSlo3 tail channels were significantly lower than those for the mSlo1 tail channels at each membrane potential examined ($P < 0.05$). For each channel type, the K_d decreased as the potential became more positive, consistent with voltage-dependent block.

The Woodhull (1973) equation can also be used to estimate the fraction of voltage drop at the blocking site measured from the intracellular side of the membrane. Analysis of the slopes in experiments like that shown in the inset to Fig. 12 D suggests that the mean distances of the effective blocking site across the membrane potential from the intracellular surface were 34 ± 2% for mSlo1 tail channels and 30 ± 2% for mslo3 tail channels, indicating no significant difference ($P = 0.14$).

DISCUSSION

In this study, we have shown that replacing the COOH-terminal tail domain region (S9–S10) of mSlo1 channels with the corresponding tail domain of mSlo3 channels conferred many of the properties of wild-type mSlo3 channels to the chimeric channels comprised of the mSlo1 core domains and mSlo3 tail domains. Compared with channels expressed from mSlo1 cores and mSlo1 tails (mSlo1 tail channels), the channels expressed from mSlo1 cores and mSlo3 tails (mSlo3 tail channels) were much less Ca^{2+} sensitive, had a higher open probability in the absence of Ca^{2+}, were less voltage-dependent, had briefer mean open times, briefer burst durations, a lower single-channel conductance, and an increased sensitivity to block by internal TEA. These observations suggest that the tail domains (S9-S10) of BK channels modulate the kinetic, conductance, and activation properties of the channel. This modification could involve both direct and indirect actions of the tail domain.

Variability among Channels

One difficulty with single-channel studies, is that there can be considerable variability in the P_O and kinetics among channels of the same apparent type under constant experimental conditions. The variability can be divided into two types: (1) variability in the P_O and/or kinetics over time for individual channels; and (2) stability in the P_O and kinetics over time for individual channels, but differences in the P_O and/or kinetics among separate channels of the same apparent type. The first type of variability has been termed wanderlust kinetics (Silberberg et al., 1996), and is controlled for in our study by analyzing those single-channel patches in which stability plots indicated relative stability of the single-channel data over time. The second type of variability, that among channels of the same type, is also often present in single-channel studies. McManus and Magleby (1991) found, for native BK channels in cultured rat skeletal muscle, that there was a wide range of P_O among channels under the same experimental conditions. Since the channels were native, it cannot be excluded that the differences in P_O arose from different splice variants (Lagrutta et al., 1994). Differences in phosphorylation and the redox state of the channels might also lead to differences in activity among channels (Wang et al., 1999; Tang et al., 2001). Hence, variability in single-channel data can be observed whether the subunits are full-length or whether they are formed from separate cores and tails, as in this study.

The second type of variability, that among channels of the same type, is compensated for in our study by presenting separate plots of data from a number of single-channel patches so that the range of variability among channels is apparent. The mean and the SEM

of the kinetic parameters determined from the individual channels are also presented to give the average response. Although the variability in the P_O and kinetics among mSlo3 tail channels under constant experimental conditions could be considerable, this variability does not alter the conclusions of our study, because the kinetics of the mSlo1 tail and mSlo3 tail channels are so characteristically different.

The S9–S10 Tail Domain of mSlo1 Is a Major Determinant of Ca^{2+} Sensitivity

Replacing the mSlo1 tail with the mSlo3 tail converted the channel from a highly sensitive Ca^{2+}- activated channel (Fig. 4 B) to a channel that was only weakly modulated by Ca^{2+} over a narrow range of P_O (Fig. 4 C). These observations are consistent with those of Schreiber et al. (1999), in which coexpression of the mSlo1 core and the mSlo3 tail yielded macroscopic currents that were Ca^{2+}-insensitive. The weak modulation of mSlo3 tail channels observed in our experiments with single-channel recording might be more difficult to detect in macroscopic currents.

Schreiber and Salkoff (1997) have suggested that BK channels contain two separable Ca^{2+} binding sites: a primary site, termed the calcium bowl located in the tail domain between S9 and S10, and a secondary site. The suggestion of a secondary site is based on their observations that mutations of the Ca^{2+} bowl alter Ca^{2+} sensitivity but not Cd^{2+} sensitivity. The secondary site is sensitive to both Ca^{2+} and Cd^{2+}, whereas the calcium bowl is sensitive only to Ca^{2+}. Consistent with these observations, preliminary experiments indicate that mSlo3 tail channels can be modulated by $Cd^{2+}{}_i$ unpublished data), suggesting that channels without a functional calcium bowl can still be activated by $Cd^{2+}{}_i$. Oberhauser et al. (1988) previously have shown that $Cd^{2+}{}_i$ can modulate the activity of $Ca^{2+}{}_i$ on BK channels, suggesting a divalent binding site in addition to the Ca^{2+} binding site. Alternatively, the secondary site may be located in the core domain. Studies using site-directed mutagenesis (Krause et al., 1996; Braun and Sy, 2001) as well as comparisons of Ca^{2+} sensitivity between BK channel splice variants (Lagrutta et al., 1994; Rosenblatt et al., 1997; Hanaoka et al., 1999) have suggested that the core domain may also contribute to Ca^{2+} sensitivity. Additional support for a secondary site are the observations of Solaro et al. (1995) that cytoplasmic Mg^{2+} modulates Ca^{2+}-dependent activation of mSlo1 by binding to a low affinity site on the channel core, and the observations of Shi and Cui (2001) that Mg^{2+} can increase BK channel activity under experimental conditions (1 mM $Ca^{2+}{}_i$), where the primary Ca^{2+} binding sites would be saturated with Ca^{2+} (Rothberg and Magleby, 1999). In the absence of Mg^{2+}, the separate Mg^{2+} site may act as a secondary Ca^{2+} binding site. Our observations that Ca^{2+} can modulate the channel (albeit weakly) when the calcium bowl is removed (by substituting the mSlo3 tail for the mSlo1 tail) can be explained by the presence of a secondary Ca^{2+} binding site on the core domain of the channel.

However, it cannot be excluded that some of the residual effects of Ca^{2+} and Cd^{2+} observed with mSlo3 tail channels may arise from the region of the mSlo3 tail replacing the calcium bowl, as this region still contains two negative charges (compared with the eight negative charges in the calcium bowl) that would be available to coordinate divalent cation binding, with negative charges located elsewhere in the channel. However, this possibility seems unlikely since wild-type mSlo3 channels show little Ca^{2+} sensitivity (Schreiber et al., 1998).

Replacing the mSlo1 tail with the mSlo3 tail reduced the Hill coefficient from ~3.2 to <40% of this value, and limited the Ca^{2+}-dependent change in P_O to a small fraction of the range of Po accessible by varying voltage. A reduced Hill coefficient could arise from a decreased number of Ca^{2+} binding sites or from a decreased efficacy of action of Ca^{2+}. Since BK channels are tetramers (Shen et al., 1994), there would be a Ca^{2+} binding site associated with the calcium bowl on the tail of each of the four α subunits of mSlo1, for a total of four primary sites, plus perhaps four additional secondary binding sites. The simplest explanation for the reduced Hill coefficient of the mSlo3 tail channels is that the number of effective Ca^{2+} binding sites is reduced due to the absence of calcium bowls in the mSlo3 tails, and that the remaining Ca^{2+} binding sites are less effective in activating the channel.

In addition to decreasing the Hill coefficient, replacing the mSlo1 tail with the mSlo3 tail increased the P_O in 0 μM $Ca^{2+}{}_i$ (+30 mV) from ~0.0005 for mSlo1 tail channels to, on average, ~0.15 for mSlo3 tail channels. Although the average P_O of mSlo3 tail channels was orders of magnitude greater than for mSlo1 tail channels under these experimental conditions, there was a wide range in the P_O among mSlo3 tail channels under these conditions, ranging from 0.0001 to 0.34. Although a number of factors could lead to differences in P_O among channels (as discussed on p. 727), an additional explanation for this variability among mSlo3 tail channels is that different numbers of mSlo3 tails may have been associated with the cores. Although excess cRNA for the mSlo3 tails, when compared with that for the core, was injected into the oocytes to reduce this possibility (MATERIALS AND METHODS), it cannot be excluded that different numbers of mSlo3 tails may have associated with some of the mSlo3 tail channels. Since functional channels cannot form from cores alone (Wei et al., 1994; Meera et al., 1997), then all of the channels we studied must have had one or more tails. Whether functional mSlo3 tail channels formed with fewer than four tails in our experiments is not known, but if so, then this uncertainty

would appear to have little effect on our conclusions, as the mSlo3 tail channels that we studied were characteristically different from the mSlo1 tail channels, and the kinetic data from the different mSlo3 tail channels appeared consistent when normalized to P_O (Fig. 8).

Our observations that the activity of mSlo3 can be considerable in 0 μM $Ca^{2+}{}_i$ at voltages (+30 mV) where the activity of mSlo1 tail channels is very low, is consistent with the results of Schreiber et al. (1999), who found that macroscopic currents from oocytes expressing mSlo3 tail channels were readily activated over a range of voltages in 0 μM Ca^{2+} that would have little effect on mSlo1 tail channels. Schreiber et al. (1999) have proposed that the tail domain of the BK channel interacts with the core domain in a manner that inhibits its channel opening, and that Ca^{2+} activates BK channels by relieving this inhibition. In terms of their hypothesis, the higher residual activity with 0 μM $Ca^{2+}{}_i$ for mSlo3 tail channels compared with mSlo1 tail channels, would reflect the weaker inhibition (due to evolutionary divergence) of mSlo3 tails on the mSlo1 core compared with that of mSlo1 tails. However, our additional observation that three of the seven mSlo3 tail channels examined had little activity under experimental conditions where mSlo1 channels would be active, are inconsistent with the inhibition hypothesis, unless there is some additional unknown factor for these particular mSlo3 channels that inhibited their activity.

Replacing the Tail of mSlo1 with the Tail of mSlo3 Reduces the Voltage Sensitivity

The decreased voltage dependence of mSlo3 tail channels was indicated by a ~28% reduction in the estimates of the effective gating charge determined from Boltzmann fits. However, mSlo1 tail channels and mSlo3 tail channels have an identical S4 transmembrane segment, which is thought to be the primary voltage sensor (Diaz et al., 1998). Recently, it has been suggested that a change in membrane potential causes a rotation of the S4 segment, such that the positively charged residues are exposed to an internal aqueous crevice at hyperpolarized potentials and to an external aqueous crevice at depolarized potentials (Bezanilla, 2000; http://pb010.anes.ucla.edu). Thus, one possible explanation for our results is that the S4 segment of mSlo3 tail channels rotates through a smaller angle, or that the position of the crevices have changed, so that the effective transfer of charge across the electric field of the membrane with the rotation of S4 is less for mSlo3 tail channels compared with mSlo1 tail channels. This could arise from either a direct or indirect (allosteric) interaction between the tail domain and the core domain. Other intracellular parts of the channel can also influence voltage sensitivity. Mutations in the S4-S5 linker can reduce voltage sensitivity (Cui and Aldrich, 2000), and comparisons of voltage dependence between BK channel splice variants suggest that regions of the core domain of the channel located intracellularly influence voltage sensitivity (Rosenblatt et al., 1997; for review see Yellen, 1998). Thus, the tail domain, which is located intracellularly, may act by direct interactions with intracellular parts of the core.

Replacing the Tail of mSlo1 with the Tail of mSlo3 Transfers the Bursting Properties of mSlo3

Replacing the mSlo1 tail with the mSlo3 tail resulted in a pronounced change in bursting kinetics, including decreases in mean burst duration, mean open time, mean number of openings per burst, and the mean duration of gaps between bursts (Fig. 8). These are the changes that would be expected, based on the differences in properties between wild-type mSlo1 and wild-type mSlo3 (Figs. 2 and 3), provided that the tail of Slo channels contributes to the bursting kinetics. Our observations together with previous observations (Lagrutta et al., 1994; Wei et al., 1994) suggest that the kinetic properties of gating are determined by both the core and the tail.

Two lines of evidence suggest that the transfer of bursting kinetics with the transfer of the tail does not arise from fundamental changes in the gating kinetics, but rather more subtle changes in the transitions rates among the states involved in the gating. First, we found no significant difference in the number of detected open or closed states after replacement of the mSlo1 tail with the mSlo3 tail (Fig. 9). Second, whereas the relative magnitudes of the various components of the dependency plots could be quite different for the two channel types, the characteristic saddle shape of the dependency plots (Rothberg and Magleby, 1998a), which reflects the effective connections among states, was still present after replacing the mSlo1 tail with the mSlo3 tail (Fig. 10). If the transfer of the tail resulted in effectively establishing new transitions pathways or new states, then such changes might be expected to change the basic shape of the dependency plots (Magleby and Song, 1992).

The transfer of bursting kinetics by replacing the mSlo1 tail with the mSlo3 tail could arise because the tail directly contributes to the gating machinery, or alternatively, because the tail serves to modulate the gating machinery in the core of the channel. The proposal of Schreiber et al. (1999) that the tail of the channel represents an evolutionary recent addition of a Ca^{2+}-dependent domain to an ancestral voltage-sensitive potassium channel, would suggest that the tail acts by modulating the gating machinery in the core. Further support for a modulatory function comes from our observations (unpublished data) that in some of the patches that were rejected from analysis because they displayed wanderlust kinetics, mSlo3 tail channels could occasionally gate in a mode with kinetics that ap-

peared similar to the normal mode activity observed in mSlo1 tail channels and wild-type mSlo1 channels, and that mSlo1 tail channels and wild-type mSlo1 channels could occasionally gate in a mode with kinetics that appeared similar to the dominant type of activity observed in mSlo3 tail channels and wild-type mSlo3 channels. Although the kinetics were too variable in these discarded experiments to perform in depth analysis, these observations suggest that some channels can gate in both mSlo1 type and mSlo3 type modes, independent of the type of tail, and for mSlo1, independent of whether the channel was expressed from a full-length clone or from separate cores and tails. On this basis, the apparent transfer of the gating kinetics with the tail may arise, not because the gating kinetics are intrinsic to the tail, but because the tail selects for and stabilizes one of the modes of gating activity intrinsic to the core. Although this conclusion is speculative for mSlo1 channels, Wang et al. (2000) have shown for nicotinic receptor channels that the ε subunit stabilizes the gating kinetics of the channel, limiting the number of kinetic modes that are available for gating.

For mSlol channels, replacing the incorrect mSlo3 tail with the correct mSlo1 tail increases mean burst duration, the mean number of openings per burst, the mean open time, and the mean gap duration for data compared at the same P_O over a wide range of P_O (Fig. 8). Interestingly, the addition of the auxiliary β_1 subunit to mSlo1 channels increases all these parameters even further (compare Fig. 8 with Fig. 6 in Nimigean and Magleby, 1999). Such a progressive shift in the bursting parameters, first by restoring the correct tail and then by adding the β_1 subunit, suggests that the fundamental energy barriers (transition rates) that are changed by replacing the mSlo3 tail with the mSlo1 tail may be changed even further by the addition of the β_1 subunit. A discussion of possible mechanisms underlying such changes in bursting kinetics is presented in Nimigean and Magleby (1999, 2000), and the background for the β1 subunit may be found in McManus et al. (1995).

Why Doesn't the Elimination of the Calcium Bowl Decrease the Number of States Detected during Gating?

Since Ca^{2+} activates BK channels, it would be expected that the binding of each additional Ca^{2+} to the channel would further change its properties, creating an additional state. If the calcium bowl contributes a major Ca^{2+} binding site to each of the four tails, as proposed (Wei et al., 1994; Schreiber and Salkoff, 1997, Schreiber et al., 1999), then eliminating the four Ca^{2+} bowls might be expected to reduce the numbers of kinetic states entered during gating. Yet, we found no reduction in the numbers of detected kinetic states during gating when the mSlo1 tails with active calcium bowls were replaced with mSlo3 tails with absent calcium bowls (Fig. 9). How is this possible?

This question can be addressed in terms of kinetic models that describe the gating of BK channels. In these discrete state Markov models, the voltage sensor in each of the four subunits of the channel can enter two conformations, and each subunit can bind a Ca^{2+}, leading to two-tiered 50-state allosteric models for the gating (Rothberg and Magleby, 1999, 2000; Cui and Aldrich, 2000; and implicated in other studies Horrigan et al., 1999; Nimigean and Magleby, 2000; Talukder and Aldrich, 2000). The 50-state models have 25 closed states on the upper tier and 25 open states on the lower tier. With 0 $Ca^{2+}{}_i$ or with all the Ca^{2+} binding sites removed, the gating in these 50-state models would be confined to the five closed and five open states without any bound Ca^{2+}. Hence, the prediction of the 50-state model is that the numbers of states detected during gating of wild-type mSlo1 channels in 0 $Ca^{2+}{}_i$ should be the same as the numbers of states detected during gating of modified BK channels in which all the Ca^{2+} binding sites have been removed, and should not exceed five open and five closed states in either case, or six open and six closed states if conformational changes in diagonal and adjacent subunits yield channels with different properties.

For a first approximation, this is found to be the case. For analysis of 1-D distributions with >500 intervals, wild-type mSlo1 channels gated among two to three detected open and three to five detected closed states in 0 $Ca^{2+}{}_i$ (Fig. 7, open symbols, in Nimigean and Magleby, 2000; and Fig. 4 in Talukder and Aldrich, 2000), and mSlo3 tail channels without calcium bowls gated among two to three detected open and three to seven detected closed states for data collected over a range of $Ca^{2+}{}_i$ (Fig. 9). The data for the mSlo1 channels in 0 $Ca^{2+}{}_i$ is consistent with the predictions of the 50-state model, as the effective numbers of states detected or entered can be less than the total number available. The detection of six closed states in a few datasets and seven closed states in one dataset for mSlo3 tail channels is greater than the maximum of five closed states typically observed and predicted by the 50-state models for channels without any Ca^{2+} binding sites.

This greater than predicted number of closed states could arise for channels with absent calcium bowls for several reasons: first, mSlo3 tail channels do display a weak Ca^{2+} dependence, so they retain some secondary Ca^{2+} binding sites that could contribute additional states; and, second, the 50-state models are too simple and, thus, under predict the numbers of states the channel can gate in. Some observations suggest that the 50-state models may need an additional tier of flicker closed states (Rothberg and Magleby, 1999, 2000). If this is the case, then the channel could gate in up to 15 states without any bound $Ca^{2+}{}_i$. Thus, our ob-

servations of mSlo3 tail channels typically gating in at least 3–4 open and 5–7 closed states does not exclude that the calcium bowl is a major Ca^{2+} binding site. In fact, gating in multiple open and closed states without a calcium bowl is just what is predicted by models for the gating of BK channels. It should also be noted that our observation of multiple open and closed states in the absence of calcium binding sites rejects simple models for gating, such as the MWC model (Monod et al., 1965), which predicts one open and one closed state under such conditions (Nimigean and Magleby, 2000; Talukder and Aldrich, 2000)

An apparent paradox concerning the 50-state models is not the numbers of states observed in the absence of the calcium bowl, but why so few of the potential 50 (or more) states are detected in the presence of Ca^{2+}_i for channels with functional calcium bowls. The maximum numbers of detected states for BK channels are typically three to four open and five to seven closed states (Fig. 9, mSlo1 tail channels; McManus and Magleby, 1988). An explanation is that each dwell-time distribution used to estimate the numbers of kinetic states must be obtained under a single set of experimental conditions (one voltage and one Ca^{2+}_i) to maintain the stability of the gating. Consequently, the effective number of states entered during data collection for any dwell-time distribution is limited because the fixed experimental conditions limit the effective sojourns to only a subset of the total states (Rothberg and Magleby, 1999, 2000). Furthermore, analysis with 50-state models shows that even for the subset of states that are entered for fixed experimental conditions, many of the exponential components generated by these states have overlapping time constants and small areas, so that only a small fraction of the total number of potential exponential components would be detected. Consequently, dwell-time distributions predicted by the 50-state models are consistent with the limited numbers of exponential components observed in the experimental data (Magleby and Rothberg, 2001).

Replacing the Tail of mSlo1 with the Tail of mSlo3 Decreases Single-channel Conductance and Facilitates the Fast Block by Internal TEA

Two observations in our study suggests that the tail domain of BK channels influences the structure of the conducting pore of the channel. Replacing the mSlo1 tail with the mSlo3 tail both reduced the single-channel conductance 14% (Fig. 11), and also facilitated the fast block of the channel by internal TEA, decreasing the apparent K_d for TEA binding by ~30% without changing the apparent electrical distance into the field at which the binding occurs (Fig. 12).

The tail domain of the channel could alter the conducting pore directly if it contributes to the intracellular part of the pore, or it could alter the access to the pore. Perhaps the tail domain is involved in forming structures at the inner part of the pore in a manner similar to the cytoplasmic β subunit-T1 assembly in voltage-dependent K^+ channels (Gulbis et al., 2000). Alternatively, the tail domain of the channel could alter the conducting pore indirectly through allosteric interactions with the core domain of the channel, which by analogy to other K^+ channels (Doyle et al., 1998) includes the selectivity filter and inner and outer vestibules of the pore. If the tail domain alters the apparent K_d for TEA binding by altering the structure at the TEA binding site, then an allosteric interaction of the tail with the core would most likely be required, as the intracellular accessed TEA binding site is located deep within the pore (Yellen et al., 1991; Doyle et al., 1998). Alterations in the apparent K_d may not require direct changes at the TEA binding site. In the *Shaker* K^+ channel, mutation in the S4–S5 loop can alter the K_d for block by internal TEA (Slesinger et al., 1993).

It is also possible that the differences in conductance and TEA block when the mSlo3 tail replaces the mSlo1 tail may be associated with differences in the gating. Perhaps the movement of the gate is restricted for mSlo3 tail channels so that the channels do not open fully, but open to a subconductance level with a conductance 14% less than the fully open mSlo1 tail channels. For Drk1 channels, openings to subconductance levels may arise from partially activated channels in which some, but not all, subunits have undergone the conformational changes required for wild-type channel opening (Chapman et al., 1997). Perhaps a similar partial activation occurs in mSlo3 tail channels.

Modular Construction of BK Channels

Long before it was known that the structure of the core domain of BK channels is similar to the structure of the superfamily of voltage-dependent K^+ channels (INTRODUCTION), Hille (1984) pointed out that even with a fixed level of Ca^{2+}_i, BK channels show an intrinsic voltage sensitivity and behave somewhat like what would be expected for delayed rectifier K^+ channels. The opening rate of BK channels increases with depolarization, and the closing rate decreases, just the properties postulated in the Hodgkin-Huxley model to explain the voltage dependence of the potassium conductance. Hille's association of BK channels with delayed rectifiers was insightful. Although Ca^{2+}_i is strictly required for BK channels to have functional activity under physiological conditions where the channels are readily activated by micromolar Ca^{2+}_i and modulated by voltage, large negative voltages can reduce channel activity to negligible levels in the presence of Ca^{2+}_i and large positive voltages can fully activate the channels in the absence of Ca^{2+}_i, suggesting an underlying voltage activated chan-

nel that is modulated by Ca^{2+}_i (Meera et al., 1996; Cui et al., 1997; Stefani et al., 1997; Diaz et al., 1998; Rothberg and Magleby, 2000; Cui and Aldrich, 2000).

Consistent with this idea, Schreiber et al. (1999) have suggested that BK channels may have evolved from an ancestral voltage-sensitive channel represented by the core domain, with the tail representing the more recent addition of a calcium-dependent modulatory domain. Our observations that removing the major Ca^{2+}_i binding sites of the channel by replacing the mSlo1 tail with the mSlo3 tail had little effect on the numbers of states detected during gating, while greatly decreasing the Ca^{2+} sensitivity, open times, burst duration, single-channel conductance, voltage dependence, and increasing sensitivity to block by TEA_i, support the concept of a modular construction of the BK channel, in which a core domain with ancestry to a voltage-dependent channel is modulated by a tail domain. Further support for the modular construction of the Slo family of channels is the observation that the mSlo1 core and mSlo1 tail domains expressed separately assemble to form channels indistinguishable from the wild-type channel (Wei et al., 1994; Meera et al., 1997), and that Slo2, another member of the Slo family of K^+ channels, which is regulated by both Ca^{2+} and Cl^-, has replaced the net positive charge of the calcium bowl region with net negative charge to form a chloride bowl (Yuan et al., 2000).

We thank Dr. Lawrence Salkoff and Dr. Matthew Schreiber for providing the cDNAs encoding wild-type mSlo1, wild-type mSlo3, the mSlo1 core, the mSlo1 tail, and the mSlo3 tail. We thank Xiang Qian for contributing some experiments for the paper.

This work was supported in part by National Institutes of Health grant AR32805 and a grant from the Muscular Dystrophy Association to K.L. Magleby.

REFERENCES

Adelman, J.P., K.Z. Shen, M.P. Kavanaugh, R.A. Warren, Y.N. Wu, A. Lagrutta, C.T. Bond, and R.A. North. 1992. Calcium-activated potassium channels expressed from cloned complementary DNAs. *Neuron*. 9:209–216.

Atkinson, N.S., G.A. Robertson, and B. Ganetzky. 1991. A component of calcium-activated potassium channels encoded by the *Drosophila slo* locus. *Science*. 253:551–555.

Armstrong, C.M., and B. Hille. 1972. The inner quaternary ammonium ion receptor in potassium channels of the node of Ranvier. *J. Gen. Physiol.* 59:388–400.

Bezanilla, F. 2000. The voltage sensor in voltage-dependent ion channels. *Physiol. Rev.* 80:R555–R592.

Bian, S., I. Favre, and E. Moczydlowski. 2001. Ca^{2+}-binding activity of a COOH-terminal fragment of the *Drosophila* BK channel involved in Ca^{2+}-dependent activation. *Proc. Natl. Acad Sci. USA*. 98: 4776–4781.

Blatz, A.L., and K.L. Magleby. 1984. Ion conductance and selectivity of single calcium-activated potassium channels in cultured rat muscle. *J. Gen. Physiol.* 84:1–23.

Braun, A.F., and L. Sy. 2001. Contribution of potential EF hand motifs to the calcium-dependent gating of a mouse brain large conductance, calcium-sensitive K^+ channel. *J. Physiol.* 533:681–695.

Butler, A., S. Tsunoda, D.P. McCobb, A. Wei, and L. Salkoff. 1993. *mSlo*, a complex mouse gene encoding "maxi" calcium-activated potassium channels. *Science*. 261:221–224.

Chapman, M.L., H.M. VanDongen, and A.M. VanDongen. 1997. Activation-dependent subconductance levels in the drk1 K channel suggest a subunit basis for ion permeation and gating. *Biophys. J.* 72:708–719.

Choi, K.L., R.W. Aldrich, and G. Yellen. 1991. Tetraethylammonium blockade distinguishes two inactivation mechanisms in voltage-activated K^+ channels. *Proc. Natl. Acad. Sci. USA*. 88:5092–5095.

Colquhoun, D., and A.G. Hawkes. 1995. The principles of the stochastic interpretation of ion-channel mechanisms. *In* Single-Channel Recording. B. Sakmann and E. Neher, editors. Plenum Press, New York. 397-482.

Colquhoun, D., and F.J. Sigworth. 1995. Fitting and statistical analysis of single-channel records. *In* Single-Channel Recording. B. Sakmann and E. Neher, editors. Plenum Press, New York. 483–587.

Conley, E.C. 1996. The Ion Channel Facts Book II. Academic Press, San Diego, CA. 778 pp.

Coronado, R., and C. Miller. 1982. Conduction and block by organic cations in a K^+-selective channel from sarcoplasmic reticulum incorporated into planar phospholipid bilayers. *J. Gen. Physiol.* 79:529–547.

Cui, J., and R.W. Aldrich. 2000. Allosteric linkage between voltage and Ca^{2+}-dependent activation of BK-type mslo1 K^+ channels. *Biochemistry*. 39:15612–15619.

Cui, J., D.H. Cox, and R.W. Aldrich. 1997. Intrinsic voltage dependence and Ca^{2+} regulation of *mslo* large conductance Ca-activated K^+ channels. *J. Gen. Physiol.* 109:647–673.

Dahl, G. 1992. The oocyte cell-cell channel assay for functional analysis of gap junction proteins. *In* Cell-Cell Interactions: A Practical Approach. B. Stevenson, D. Paul, and W. Gallin, editors. Oxford University Press, London/New York. 143–165.

Diaz, L., P.J. Meera, E. Amigo, E. Stefani, O. Alvarez, L. Toro, and R. Latorre. 1998. Role of the S4 segment in a voltage-dependent calcium-sensitive potassium (h*Slo*) channel. *J. Biol. Chem.* 273: 32430–32436.

Doyle, D.A., J. Morais Cabral, R.A. Pfuetzner, A. Kuo, J.M. Gulbis, S.L. Cohen, B.T. Chait, R. MacKinnon. 1998. The structure of the potassium channel: molecular basis of K^+ conduction and selectivity. *Science*. 280:69–77.

Dworetzky, S.I., J.T. Trojnacki, and V.K. Gribkoff. 1994. Cloning and expression of a human large-conductance calcium-activated potassium channel. *Brain Res. Mol. Brain Res.* 27:189–193.

Fredkin, D.R., M. Montal, and J.A. Rice. 1985. Identification of aggregated Markovian models: application to the nicotinic acetylcholine receptor. Proc. Berkeley Conf. in Honor of Jerzy Neyman and Jack Kiefer. 269–289.

Golowasch, J., A. Kirkwood, and C. Miller. 1986. Allosteric effects of Mg^{2+} on the gating of Ca^{2+}-activated K^+ channels from mammalian skeletal muscle. *J. Exp. Biol.* 124:5–13.

Gulbis, J.M., M. Zhou, S. Mann, and R. MacKinnon. 2000. Structure of the cytoplasmic β subunit-T1 assembly of voltage-dependent K^+ channels. *Science*. 289:123–127.

Hamill, O.P., A. Marty, E. Neher, B. Sakmann, and F.J. Sigworth. 1981. Improved patch clamp techniques for high-resolution current recording from cells and cell-free membrane patches. *Pflügers Archiv.* 391:85–100.

Hanaoka, K., J.M. Wright, I.B. Cheglakov, T. Morita, and W.B. Guggino. 1999. A 59 amino acid insertion increases Ca^{2+} sensitivity of rbslo1, a Ca^{2+}-activated K^+ channel in renal epithelia. *J. Membr. Biol.* 172:193–201.

Hille, B. 1984. Ionic Channels of Excitable Membranes. Sinauer Associates, Inc., Sunderland, MA. 426 pp.

Horrigan, F.T., J. Cui, and R.W. Aldrich. 1999. Allosteric voltage

gating of potassium channels I. *mSlo* ionic currents in the absence of Ca^{2+}. *J. Gen. Physiol.* 114:277–304.

Hudspeth, A.J., and R.S. Lewis. 1988. Kinetic analysis of voltage- and ion-dependent conductances in saccular hair cells of the bull-frog, Rana catesbeiana. *J. Physiol.* 400:237–274.

Jiang, G.J., M. Zidanic, R.L. Michaels, T.H. Michael, C. Griguer, and P.A. Fuchs. 1997. Cslo encodes calcium-activated potassium channels in the chick's cochlea. *Proc. R. Soc. Lond. B. Biol. Sci.* 264:731–737.

Kaczorowski, G.J., H.G. Knaus, R.J. Leonard, O.B. McManus, and M.L. Garcia. 1996. High-conductance calcium-activated potassium channels: structure, pharmacology, and function. *J. Bioenerg. Biomembr.* 28:255–267.

Keller, B.U., M.S. Montal, R.P. Hortshorne, and M. Montal. 1990. Two-dimensional probability density analysis of single channel currents from reconstituted acetylcholine receptors and sodium channels. *Arch. Biochem. Biophys.* 276:47–54.

Krause, J.D., C.D. Foster, and P.H. Reinhart. 1996. *Xenopus laevis* oocytes contain endogenous large conductance Ca^{2+}-activated K^+ channels. *Neuropharmacology.* 35:1017–1022.

Lagrutta, A., K.R.A. Shen, R.A. North, and J.P. Adelman. 1994. Functional differences among alternatively spliced variants of *slowpoke*, a *Drosophila* calcium-activated potassium channel. *J. Biol. Chem.* 269:20347–20351.

Latorre, R. 1994. Molecular workings of large conductance (maxi) Ca^{2+}-activated K^+ channels. *In* Handbook of Membrane Channels: Molecular and Cellular Physiology. C. Peracchia, editor. Academic Press, New York. 79–102.

Magleby, K.L., and B.S. Pallotta. 1983a. Calcium dependence of open and shut interval distributions from calcium-activated potassium channels in cultured rat muscle. *J. Physiol.* 344:585–604.

Magleby, K.L., and B.S. Pallotta. 1983b. Burst kinetics of single calcium-activated potassium channels in cultured rat muscle. *J. Physiol.* 344:605–623.

Magleby, K.L., and L. Song. 1992. Dependency plots suggest the kinetic structure of ion channels. *Proc. R. Soc. Lond. B. Biol. Sci.* 249: 133–142.

Magleby, K.L., and B.S. Rothberg. 2001. Cooperative allosteric gating for voltage and Ca^{2+}-activation of large conductance Ca^{2+}-activated K^+ (BK) channels. *Biophys. J.* 80:222A. (Abstr.)

McCobb, D.P., N.L. Fowler, T. Featherstone, C.J. Lingle, M. Saito, J.E. Krause, and L. Salkoff. 1995. A human calcium-activated potassium channel gene expressed in vascular smooth muscle. *Am. J. Physiol.* 269:H767–H777.

McManus, O.B. 1991. Calcium-activated potassium channels: regulation by calcium. *J. Bioenerg. Biomembr.* 23:537–560.

McManus, O.B., and K.L. Magleby. 1988. Kinetic states and modes of single large-conductance calcium-activated potassium channels in cultured rat skeletal muscle. *J. Physiol.* 402:79–120.

McManus, O.B., and K.L. Magleby. 1991. Accounting for the Ca^{2+}-dependent kinetics of single large-conductance Ca^{2+}-activated K^+ channels in rat skeletal muscle. *J. Physiol.* 443:739–777.

McManus, O.B., L.M. Helms, L. Pallanck, B. Ganetzky, R. Swanson, and R.J. Leonard. 1995. Functional role of the β subunit of high conductance calcium-activated potassium channels. *Neuron.* 14: 645–650.

Meera, P., M. Wallner, Z. Jiang, and L. Toro. 1996. A calcium switch for the functional coupling between α (h*slo*) and β subunits ($K_{V,Ca}$ β) of maxi K channels. *FEBS Lett.* 382:84–88.

Meera, P., M. Wallner, M. Song, and L. Toro. 1997. Large conductance voltage- and calcium-dependent K^+ channel, a distinct member of voltage-dependent ion channels with seven N-terminal transmembrane segments (S0-S6), an extracellular N terminus, and an intracellular (S9-S10) C terminus. *Proc. Natl. Acad. Sci. USA.* 94:14066–14071.

Monod, J., J. Wyman, and J.-P. Changeux. 1965. On the nature of allosteric transitions: a plausible model. *J. Mol. Biol.* 12:88–118.

Moss, B.L., and K.L. Magleby. 2000. BK channel carboxyl terminal tail domain can modulate gating properties and conductance. *Biophys. J.* 78:92A (Abstr.)

Moss, B.L., S.D. Silberberg, C.M. Nimigean, and K.L. Magleby. 1999. Ca^{2+}-dependent gating mechanisms for *dSlo*, a large-conductance Ca^{2+}-activated K^+ (BK) channel. *Biophys. J.* 76:3099–3117.

Navaratnam, D.S., T.J. Bell, T.D. Tu, E.L. Cohen, and J.C. Oberholtzer. 1997. Differential distribution of Ca^{2+}-activated K^+ channel splice variants among hair cells along the tonotopic axis of the chick cochlea. *Neuron.* 19:1077–1085.

Nelson, M.T., H. Cheng, M. Rubart, L.F. Santana, A.D. Bonev, H.J. Knot, and W.J. Lederer. 1995. Relaxation of arterial smooth muscle by calcium sparks. *Science.* 270:633–637.

Nimigean, C.M., and K.L. Magleby. 1999. The β subunit increases the $Ca2^+$ sensitivity of large conductance Ca^{2+}-activated potassium channels by retaining the gating in the bursting states. *J. Gen. Physiol.* 113:425–439.

Nimigean, C.M., and K.L. Magleby. 2000. Functional coupling of the β1 subunit to the large conductance Ca^{2+}-activated K^+ channel in the absence of Ca^{2+}: increased Ca^{2+} sensitivity from a Ca^{2+}-independent mechanism. *J. Gen. Physiol.* 115:719–734.

Oberhauser, A., O. Alvarez, and R. Latorre. 1988. Activation by divalent cations of a Ca^{2+}-activated K^+ channel from skeletal muscle membrane. *J. Gen. Physiol.* 92:67–86.

Pallanck, L., and B. Ganetzky. 1994. Cloning and characterization of human and mouse homologs of the *Drosophila* calcium-activated potassium channel gene, *slowpoke*. *Hum. Mol. Genet.* 3:1239–1243.

Petersen, O.H., and Y. Maruyama. 1984. Calcium-activated potassium channels and their role in secretion. *Nature.* 307:693–696.

Robitaille, R., M.L. Garcia, G.J. Kaczorowski, and M.P. Charlton. 1993. Functional colocalization of calcium and calcium-gated potassium channels in control of transmitter release. *Neuron.* 11: 645–655.

Rosenblatt, K.P., Z.P. Sun, S. Heller, and A.J. Hudspeth. 1997. Distribution of Ca^{2+}-activated K^+ channel isoforms along the tonotopic gradient of the chicken's cochlea. *Neuron.* 19:1061–1075.

Rothberg, B.S., and K.L. Magleby. 1998a. Kinetic structure of large-conductance Ca^{2+}-activated K^+ channels suggests that the gating includes transitions through intermediate or secondary states: A mechanism for flickers. *J. Gen. Physiol.* 111:751–780.

Rothberg, B.S., and K.L. Magleby. 1998b. Investigating single-channel gating mechanisms through analysis of two-dimensional distributions. *Methods Enzymol.* 293:437–456.

Rothberg, B.S., and K.L. Magleby. 1999. Gating kinetics of single-large-conductance Ca^{2+}-activated K^+ channels in high Ca^{2+} suggest a two-tiered allosteric gating mechanism. *J. Gen. Physiol.* 114: 95–124.

Rothberg, B.S., and K.L. Magleby. 2000. Voltage and Ca^{2+} activation of single large-conductance Ca^{2+}-activated channels described by a two tier allosteric gating mechanism. *J. Gen. Physiol.* 116:75–99.

Rothberg, B.S., R.A. Bello, L. Song, and K.L. Magleby. 1996. High Ca^{2+} concentrations induce a low activity mode and reveal Ca^{2+}-independent long shut intervals in BK channels from rat muscle. *J. Physiol.* 493:673–689.

Rothberg, B.S., R.A. Bello, and K.L. Magleby. 1997. Two-dimensional components and hidden dependencies provide insight into ion channel gating mechanisms. *Biophys. J.* 72:2524–2544.

Schreiber, M., and L. Salkoff. 1997. A novel calcium-sensing domain in the BK channel. *Biophys. J.* 73:1355–1363.

Schreiber, M., A. Wei, A. Yuan, J. Gaut, M. Saito, and L. Salkoff. 1998. Slo3, a novel pH-sensitive K^+ channel from mammalian spermatocytes. *J. Biol. Chem.* 273:3509–3516.

Schreiber, M., A. Yuan, and L. Salkoff. 1999. Transplantable sites confer calcium sensitivity to BK channels. *Nat. Neurosci.* 2:416–421.

Shen, K.-Z., A. Lagrutta, N.W. Davies, N.B. Standen, J.P. Adelman, and R.A. North. 1994. Tetraethylammonium block of *slowpoke* calcium-activated potassium channels expressed in *Xenopus* oocytes: evidence for tetrameric channel formation. *Pflügers Arch.* 426: 440–445.

Shi, J., and J. Cui. 2001. Intracellular Mg^{2+} enhances the function of BK-type Ca^{2+} activated K^+ channels. *Biophys. J.* 80:221A. (Abstr.)

Sigworth, F.J., and S.M. Sine. 1987. Data transformations for improved display and fitting of single-channel dwell time histograms. *Biophys. J.* 52:1047–1054.

Silberberg, S.D., A. Lagrutta, J.P. Adelman, and K.L. Magleby. 1996. Wanderlust kinetics and variable Ca^{2+}-sensitivity of *dSlo*, a large conductance Ca^{2+}-activated K^+ channel, expressed in oocytes. *Biophys. J.* 70:2640–2651.

Slesinger, P.A., Y.N. Jan, and L.Y. Jan. 1993. The S4-S5 loop contributes to the ion-selective pore of potassium channels. *Neuron.* 11: 739–749.

Solaro, C., C. Nelson, A. Wei, L. Salkoff, and C. Lingle. 1995. Cytoplasmic Mg^{2+} modulates Ca^{2+}-dependent activation of mSlo by binding to a low affinity site on the channel core. *Biophys. J.* 68: A30. (Abstr.)

Stefani, E., M. Ottolia, F. Noceti, R. Olcese, M. Wallner, R. Latorre, and L. Toro. 1997. Voltage-controlled gating in a large conductance Ca^{2+}-sensitive K^+ channel (hslo). *Proc. Natl. Acad. Sci. USA.* 94:5427–5431.

Taglialatela, M., J.A. Drewe, G.E. Kirsch, M. De Biasi, H.A. Hartmann, and A.M. Brown. 1993. Regulation of K^+/Rb^+ selectivity and internal TEA blockade by mutations at a single site in K^+ pores. *Pflügers Arch.* 423:104–112.

Talukder, G., and R.W. Aldrich. 2000. Complex voltage-dependent behavior of single unliganded calcium-sensitive potassium channels. *Biophys. J.* 78:761–772.

Tang, X.D., H. Daggett, M. Hanner, M.L. Garcia, O.B. McManus, N. Brot, H. Weissbach, and S.H. Heinemann. 2001. Oxidative regulation of large conductance calcium-activated potassium channels. *J. Gen. Physiol.* 117:253–274.

Tseng-Crank, J., C.D. Foster, J.D. Krause, R. Mertz, N. Godinot, T.J. DiChiara, and P.H. Reinhart. 1994. Cloning, expression, and distribution of functionally distinct Ca^{2+}-activated K^+ channel isoforms from human brain. *Neuron.* 13:1315–1330.

Wallner, M., P. Meera, and L. Toro. 1996. Determinant for β-subunit regulation in high-conductance voltage-activated and Ca^{2+}-sensitive K^+ channels: an additional transmembrane region at the N terminus. *Proc. Natl. Acad. Sci. USA.* 93:14922–14927.

Wang, H.L., K. Ohno, M. Milone, J.M. Brengman, A. Evoli, A.P. Batocchi, L.T. Middleton, K. Christodoulou, A.G. Engel, S.M. Sine. 2000. Fundamental gating mechanism of nicotinic receptor channel revealed by mutation causing a congenital myasthenic syndrome. *J. Gen. Physiol.* 116:449–462.

Wang, J., Y. Zhou, H. Wen, and I.B. Levitan. 1999. Simultaneous binding of two protein kinases to a calcium-dependent potassium channel. *J. Neurosci.* 19:R1–R7.

Wei, A., C. Solaro, C. Lingle, and L. Salkoff. 1994. Calcium sensitivity of BK-type K_{Ca} channels determined by a separable domain. *Neuron.* 13:671–681.

Woodhull, A.M. 1973. Ionic blockage of sodium channels in nerve. *J. Gen. Physiol.* 61:687–708.

Wu, Y.C., J.J. Art, M.B. Goodman, and R. Fettiplace. 1995. A kinetic description of the calcium-activated potassium channel and its application to electrical tuning of hair cells. *Prog. Biophys. Mol. Biol.* 63:131–158.

Yang, X.-C., and F. Sachs. 1989. Block of stretch-activated ion channels in *Xenopus* oocytes by gadolinium and calcium ions. *Science.* 243:1068–1071.

Yellen, G. 1998. The moving parts of voltage-gated ion channels. *Q. Rev. Biophys.* 31:239–295.

Yellen, G., M.E. Jurman, T. Abramson, and R. MacKinnon. 1991. Mutations affecting internal TEA blockade identify the probable pore-forming region of a K^+ channel. *Science.* 251:939–942.

Yuan, A., M. Dourado, A. Butler, N. Walton, A. Wei, and L. Salkoff. 2000. SLO-2, a K^+ channel with an unusual Cl^- dependence. *Nat. Neurosci.* 3:771–779.